Tracing marine cryptotephras in the North Atlantic during the Last Glacial Period: Improving the North Atlantic marine tephra framework

Peter M. Abbott[1,2,3,*], Adam J. Griggs[1], Anna J. Bourne[1,4], Mark R. Chapman[5], Siwan M. Davies[1]

[1]Department of Geography, College of Science, Swansea University, Singleton Park, Swansea, SA2 8PP, UK
[2]School of Earth and Ocean Sciences, Cardiff University, Park Place, CF10 3AT, Cardiff, UK
[3]Institute of Geological Sciences and Oeschger Center for Climate Change Research, University of Bern, Baltzerstrasse 1+3, Bern 3012, Switzerland
[4]Geography and Environment, University of Southampton, University Road, Southampton, SO17 1BJ, UK
[5]School of Environmental Sciences, University of East Anglia, Norwich Research Park, NR4 7TJ, UK

*Corresponding author (abbottp@cardiff.ac.uk)

Abstract

Tephrochronology is increasingly being recognised as a key tool for the correlation of disparate palaeoclimatic archives, underpinning chronological models and facilitating climatically independent comparisons of climate proxies. Tephra frameworks integrating both distal and proximal tephra occurrences are essential to these investigations providing key information on their spatial distributions, geochemical signatures, eruptive sources as well as any available chronological and/or stratigraphic information. Frameworks also help to avoid mis-correlation of horizons and provide important information on volcanic history. Here we present a comprehensive framework of 14 tephra horizons from North Atlantic marine sequences spanning 25-60 ka BP. Horizons previously discovered as visible or coarse-grained deposits have been combined with 11 newly recognised volcanic events, identified through the application of cryptotephra identification and characterisation methods to a wide network of marine sequences. Their isochronous integrity has been assessed using their physical characteristics. All horizons originated from Iceland with the vast majority having a basaltic composition sourced from the Grímsvötn, Kverkfjöll, Hekla/Vatnafjöll and Katla volcanic

systems. New occurrences, improved stratigraphic placements and a refinement of the geochemical signature of the NAAZ II are reported and the range of the FMAZ IV has been extended. In addition, several significant geochemical populations that further investigations could show to be isochronous are reported. This tephra framework provides the foundation for the correlation and synchronisation of these marine records to the Greenland ice-cores and European terrestrial records to investigate the phasing, rate, timing and mechanisms controlling the rapid climate changes that characterised the last glacial period.

Keywords: Quaternary; palaeoceanography; tephrochronology; North Atlantic; tephra framework; marine cores

1. Introduction

Tephrochronology, the use of volcanic ash deposits as tie-lines between disparate palaeoclimatic records, is increasingly being utilised as a key geochronological tool for reconstructing the timing and phasing of past climatic events (e.g. Lowe, 2011; Lowe et al., 2012; Lane et al., 2013; Davies, 2015). This upsurge is directly linked to advances in cryptotephra analysis, which has dramatically increased the number of potential tie-lines and led to the compilation of regional tephra frameworks that underpin correlations and are key datasets for future tephrochronological studies (e.g. Lowe et al., 2008; Tyron et al., 2009; Zanchetta et al., 2011; Davies et al., 2012; Abbott and Davies, 2012; Lowe et al., 2015). Tephrostratigraphical frameworks typically include a compilation of key information relating to the tephra horizons within them, including their spatial extent, based on preservation within proxy records, tephra shard concentrations, glass shard composition and eruptive source alongside chronological and stratigraphic information (e.g. Davies et al., 2014; Bourne et al., 2015; Matthews et al., 2015). The most comprehensive frameworks include both distal and proximal tephra findings, visible and cryptotephra tephra occurrences and combine newly discovered data with previously published deposits. Integrating all this information can provide valuable frameworks for the volcanic history of a region and provide key reference tools for future studies. Distal archives are often more complete than proximal records, that are prone to removal or burial of deposits, while proximal archives can often record more information regarding eruptions, such as their full geochemical evolution. In addition, developing the most comprehensive tephra frameworks will help to reduce instances of mis-correlation which can occur if volcanic regions produce multiple, closely-timed eruptions with similar geochemical compositions (e.g. Bourne et al., 2013).

For the North Atlantic region a number of detailed frameworks spanning a range of time-intervals are currently available. For example, Gudmundsdottir et al. (2016) provides a proximal framework of Icelandic eruptions during the Holocene, Blockley et al. (2014) summarises the European tephra stratigraphy over the last glacial cycle and Davies et al. (2014) provides an integrated framework of MIS 5 tephras in Greenland ice-cores and North Atlantic marine records. The tephra framework for the Greenland ice-cores has significantly expanded in recent years (e.g. Mortensen et al., 2005; Abbott and Davies, 2012; Davies et al., 2014), in particular over the MIS 2-3 period (Bourne et al., 2015), highlighting the value of exploring these distal archives. In comparison, however, a limited number of tephra horizons have been identified in North Atlantic marine records spanning MIS 2-3 (see Haflidason et al., 2000; Wastegård et al., 2006; Section 2). This is despite considerable advances in distal tephrochronology and the high potential for a tephra framework from these sequences to be used to establish correlations to the Greenland ice-cores and European terrestrial records. Such correlations could help answer key questions regarding the relative timing of atmospheric and oceanic changes associated with the rapid climatic events, that punctuated the region during the last glacial period (e.g. NGRIP Members, 2004; Bond et al., 1993; Martrat et al., 2007; Hall et al., 2011; Zumaque et al., 2012; Henry et al., 2016).

Here we present a tephra framework for North Atlantic marine records spanning MIS 2-3, which is underpinned by our investigations of an extensive core network (Figure 1) using recently developed cryptotephra identification methods (Abbott et al., submitted). Prior studies are also reviewed (Section 2) and previously identified isochronous horizons are integrated with our new cryptotephra discoveries. This represents the most concerted attempt to improve the tephra framework for the North Atlantic and overall a framework of 14 marine tephra horizons between 25-60 ka BP has been defined (Figure 2). This framework significantly enhances the potential to establish further correlations within the North Atlantic Ocean as well as to ice-core and terrestrial records.

2. Prior North Atlantic Tephra Investigations between 25-60 ka BP

It was highlighted earlier that tephra frameworks should integrate all isochronous tephra deposits from a region and, as such, the framework presented in this work integrates our new discoveries alongside previously published data from multiple cores sites from the North Atlantic (green sites on Figure 1). Within these prior tephrochronological studies of the MIS 2-3 period several isochronous tephra horizons have been identified, i.e. North Atlantic Ash Zone II (NAAZ II), Faroe Marine Ash Zone (FMAZ) II and FMAZ IV. Reviewing the literature does, however, highlight some of the challenges associated with determining the isochronous nature of deposits and the limitations of earlier studies that only focused on the coarse fraction (>150 μm) of the sediments. These were the major factors driving the development of a procedure for isolating fine-grained cryptotephras (down to 25 μm diameter) and interpreting transportation and depositional processes (e.g. Abbott et al., 2011, submitted; Davies et al., 2014; Griggs et al., 2014). The latter is essential for determining the isochronous nature of fine-grained, cryptotephra deposits for which macro-sedimentary evidence cannot be utilised to determine the relative influence of primary and secondary processes. These methods were utilised by Abbott et al. (2016) to identify three previously undocumented MIS 2-3 volcanic events within a core retrieved from the Goban Spur (see Section 4 for details) and are more widely applied in this study.

The first MIS 3 tephra deposit to be recognised in the North Atlantic was NAAZ II, first identified by Bramlette and Bradley (1941) and later described by Ruddiman and Glover (1972). This is a complex ash zone composed of the products of several Icelandic eruptions (see Section 4.1.1) with rhyolitic material from one eruption (II-RHY-1) the most widespread, being traced into multiple marine cores and the Greenland ice-cores (e.g. Kvamme et al., 1989; Lacasse et al., 1996; Haflidason et al., 2000; Austin et al., 2004; Grönvold et al., 1995; Zielinski et al., 1997; Svensson et al., 2008). This widespread nature gives rise to a key tie-line between North Atlantic marine records and the Greenland ice-cores within the North Atlantic tephra framework (Austin and Abbott, 2010).

The FMAZs are a series of ash zones identified in cores around the Faroe Islands region, and three, II, III and IV, were deposited during MIS 2-3. Two of these, FMAZ II and IV, have isochronous characteristics and are integrated within the framework (Figures 1 and 2; Rasmussen et al., 2003; Wastegård et al., 2006; Wastegård and Rasmussen, 2014; Griggs et al., 2014). FMAZ II was described by Wastegård et al. (2006) as a visible horizon and was suggested to be a widespread primary airfall deposit. The FMAZ II was subsequently traced into the NGRIP ice-core by Davies et al. (2008) (NGRIP 1848 m; 26,740 ± 390 yr b2k), providing a clear demonstration of the high potential for ice-marine correlations between the Greenland ice-cores and North Atlantic marine sequences during the 25-60 ka BP period. FMAZ IV was first described by Wastegård and Rasmussen (2014) as a layer up to 20 cm thick deposited shortly after warming related to Dansgaard-Oeschger (DO) event 12. Due to its homogenous composition and micro-sedimentary features (Griggs et al., 2014, 2015) it has been interpreted as a primary airfall deposit.

FMAZ III, identified as a thick relatively scattered zone of tephra in the Faroes cores, was also thought to have a correlative in the NGRIP core (NGRIP 2066.95 m; 38,122 ± 723 yr b2k; Davies et al., 2010). However, Bourne et al. (2013) subsequently identified a series of closely-spaced tephra horizons in the NGRIP and NEEM ice-cores around NGRIP 2066.95 m, many with geochemical compositions that fall within the wide geochemical envelope of FMAZ III. This highlighted the complexity of the period and demonstrated that the suggested correlation was inappropriate and did not represent an ice-marine tie-line (Bourne et al., 2013). Bourne et al. (2013) and Griggs et al. (2014) both suggested that FMAZ III formed through the amalgamation of tephra due to several closely spaced volcanic events and low sedimentation rates at the core sites and as such is not incorporated in the marine tephra framework.

Early studies of North Atlantic tephra mainly focused on investigating visible tephra horizons or tephra shards present within the coarse fraction of the sediment (i.e. >150 μm diameter). This may have created a bias towards the identification of horizons from large scale eruptions and/or horizons not deposited via primary airfall (Brendryen et al., 2010; Abbott et al., 2011). The study of Lackschewitz and Wallrabe-Adams (1997) highlights the limitation of this approach. Several ash zones above NAAZ II were identified within and correlated between a series of cores from the Reykjanes Ridge, however, most of these deposits have heterogeneous geochemical compositions and in general coincide with distinct peaks in ice-rafted debris (IRD). Based on these factors Lackschewitz and Wallrabe-Adams (1997) concluded that this material was transported to the sites via iceberg rafting. This process could have significantly delayed the deposition of these deposits and, as such, they do not represent isochronous marker horizons and are not incorporated in the marine tephra framework. The only deposit with isochronous characteristics was the VZ 1x peak, a discrete high concentration peak within VZ 1 in the SO82-5 core, with a homogenous composition and no coeval IRD peak. This horizon was subsequently correlated to FMAZ II by Wastegård et al. (2006) (Figure 2).

Voelker and Haflidason (2015) utilised the coarse sediment fraction to define a high-resolution tephrochronology for the last 86 ka from the southern Greenland Sea PS2644 core. This sequence was interpreted as containing a record of 68 volcanic events between ~25-60 ka BP based on the geochemical analysis of glass shards from 28 depths in the core. The volcanic events, however, are sometimes defined based on a limited number of geochemical analyses with multiple geochemical populations/events often identified at the same depth. According to protocols for assessing deposits this could be indicative of deposition via iceberg rafting and/or secondary depositional processes (Abbott et al., submitted), however, while these processes were acknowledged a distinction between tephra deposited via primary or secondary process is often not made. This may have led to the overreporting of the number of isochronous deposits present and, as such, these volcanic events are not incorporated into the North Atlantic tephra framework presented here. However, it is important to note these findings as a reappraisal of these deposits together with IRD evidence may well reveal the presence of dominant populations and valuable isochrons in the future.

3. Methodology

3.1 Detecting, characterising and correlating cryptotephra deposits

A widespread network of North Atlantic cores was investigated (Figure 1) and we applied the consistent methodological approach for cryptotephra identification outlined in Abbott et al. (submitted). Following preliminary low-resolution analysis high-resolution glass shard concentration profiles were gained from the core deposits. The major element composition of peaks in glass shard concentrations were characterised using electron-probe micro-analysis (EPMA) with at least 20-40 individual shards from each deposit analysed (see Abbott et al., submitted for full description). For all analysis and data comparison the major element data were normalised to an anhydrous basis, i.e. 100 % total oxides, however, the raw geochemical data are provided in the Supplementary Data alongside secondary standard analyses (Table S12). Potential sources for geochemical populations and tephra horizons were explored through graphical comparison of the composition of individual shards with glass and whole rock analyses from proximal Holocene Icelandic deposits from the three different rock suites and specific volcanic systems. We acknowledge that some centres may have geochemically evolved or not been productive during the last glacial period, therefore, the potential sources proposed here could be revised.

Potential cross-correlations between all the isochronous horizons and significant geochemical populations in cores within the network and other marine records were explored using statistical comparisons of their average geochemical signature and graphical comparisons on bivariate plots. The similarity coefficient function (SC) of Borchardt et al. (1972) was utilised to construct a matrix for all these comparisons (Table S13). Twenty-five of the comparisons returned SC values greater than 0.97, which implies there are strong similarities in the geochemical signatures and further assessment was required to determine if they are correlatives. A combination of three main factors were used to rule out most of these comparisons as potential correlatives; large stratigraphic discrepancies, subtle geochemical differences, and occurrence at different depths in the same core sequence. Despite the majority being ruled out, upon further assessment two of the comparisons with high SC values were found to have very strong geochemical similarities and consistent stratigraphic positions and are suggested as correlations between marine sequences in the network (see Section 4).

3.2 Assessing the isochronous nature of cryptotephra deposits

Several of the deposits reported here have been described in Abbott et al. (submitted) as illustrative examples for assessing the dominant controls on tephra deposition in the North Atlantic region. We synthesise these results in a framework of tephra deposits that represent isochronous marker horizons identified using protocols set out in Griggs et al. (2014) and Abbott et al. (submitted). The key characteristics used to define isochronous horizons are: (i) a clear peak in the shard concentration profile that can be used as the isochron position and (ii) a homogenous geochemical population, indicative of material deriving from a single volcanic eruption. The deposit type scheme outlined in Abbott et al. (submitted) is utilised to assess deposits as it accounts for variability in geochemical signatures and shard concentration profiles observed for North Atlantic marine tephra deposits. While Type 1 and 3 deposits are typically characterised by single homogenous populations there is greater variability and complexity in the geochemical signatures of Type 2 deposits. For the latter a larger number, up to 60 but typically >30, of single-grain major element analyses were gained. These were graphically assessed to explore the relative homo/heterogeneity of deposits, define homogenous populations that may have derived from single eruptions, quantify their relative dominance within the deposits and categorise them as Type 2A or Type 2B deposits. Outliers were defined as analyses that were not consistently associated with a defined population. For some deposits where populations were not defined all analyses could be categorised as 'outliers', however, in these situations shards were grouped based on affinities to the Icelandic rock suites.

3.3 Age and stratigraphic constraints

The timing of deposition for each tephra deposit is given based on the available climatostratigraphy for the specific core within which the horizons were isolated (Table 1). For some records, there is strong stratigraphic control based on proxy records from the cores that record the DO events which characterised the North Atlantic region during the last glacial period, e.g. MD04-2822 and MD04-2829CQ. However, for other cores, e.g. MD99-2251 and GIK23415-9, the stratigraphic frameworks are not as distinct with deposits from the Heinrich Events providing the best stratigraphic control. Due to uncertainties in the relative timing of closely spaced horizons not identified in the same core sequence the stratigraphic relationships presented in Figure 2 should be treated with caution, e.g. the cluster of horizons that have been identified in various cores around the H4 event (Figure 2). Further investigations of these horizons, such as their tracing into other sequences, may help to refine the sequence of the volcanic events in the future.

4. North Atlantic Tephra Framework

An improved marine tephra framework for the North Atlantic between 25-60 kyr BP is presented in Figure 2 and Table 1. Overall, a framework of 14 isochronous horizons can be defined, including 8 new isochronous horizons presented for the first time, 3 cryptotephra deposits identified in MD04-2820CQ by Abbott et al. (2016) and 3 previously published deposits (NAAZ II, FMAZ IV and FMAZ II). This represents a significant increase in the number of tephra marker horizons that could be utilised for the correlation of records during this period.

With the exception of NAAZ II (II-RHY-1) and MD04-2820CQ 497-498 cm, all tephras in the framework are basaltic in composition and originated from Iceland, specifically from the Grímsvötn, Kverkfjöll, Hekla/Vatnafjöll and Katla volcanic systems (Table 1). The most widespread isochronous horizon in the framework is the NAAZ II (II-RHY-1) (Figures 3 and 4). The wide distribution and importance of this horizon had been established in prior studies, however, here we have isolated it in more sequences, gained greater control on the timing of deposition, with peaks in shard concentration determined at a 1 cm resolution, and provided an improved geochemical signature for the horizon (Section 4.1.1). The geographical range of the previously identified FMAZ IV can be expanded, to a limited extent, from the Faroe Islands region to the Norwegian Sea following its identification in MD95-2010 (Figure 5; Section 4.1.2).

Within our network only two cores, MD04-2822 and MD04-2829CQ, exclusively preserved isochronous Type 1 deposits (Figures 6a and 6b). New isochronous horizons were also identified in two further cores, MD99-2251 and GIK23415-9, alongside other deposits without clear isochronous characteristics, i.e. Type 2B and Type 4 deposits (Figures 7a and 8a), which can be attributed to temporal variability in the processes controlling tephra deposition at these sites (see Abbott et al., submitted). Further details regarding all the isochronous horizons are provided in Section 4.1 in chronological order from the oldest to the youngest horizon.

The Type 2B and Type 4 horizons are not overlooked though as analysis showed that within many of these deposits significant homogenous geochemical populations could be isolated (Figures 7b and 8b; Table 1). These populations are presented alongside the framework of isochronous horizons as their geochemical homogeneity suggests that they were derived from single volcanic events, but, at present, questions remain over their depositional origin and isochronous nature. Further investigations, however, may permit their integration into the regional tephra framework and this is discussed further in Section 4.2.

4.1 Isochronous Horizons

4.1.1 NAAZ II

NAAZ II is a crucial deposit within the North Atlantic marine tephra framework and it has been identified at nine sites within our network as a clear peak in rhyolitic material and at 6 sites basaltic/intermediate material was also present. Based on occurrences of NAAZ II in several North Atlantic sites this ash zone was defined as being composed of five geochemical populations, one rhyolitic (II-RHY-1) and four basaltic (II-THOL-1, II-THOL-2, II-THOL-3 and II-TAB-1) by Kvamme et al. (1989).

Shards from the peaks in rhyolitic material at the 9 sites have a consistent homogenous transitional alkali rhyolitic composition (Figure 3ai and 4b; Table S2). In comparison to prior characterisations of NAAZ II from several North Atlantic marine cores strong similarities can be observed for some elements, e.g. FeO and CaO (Figure 3bi) but some offsets are apparent for other elements, e.g. Na_2O and SiO_2 (Figure 3bii). These differences are reflected in similarity coefficient comparisons (Table S2) and are consistent with sodium loss affecting the older EPMA analyses, particularly for the analyses from Kvamme et al. (1989), and are highly unlikely to indicate a different source for the material (Hunt and Hill, 1993; Kuehn et al., 2011). Therefore, the nine deposits in this network can be correlated to the II-RHY-1 component of NAAZ II. These new analyses provide an up-to-date composition for this component and highlight that data quality must be considered when assessing correlations between datasets, especially for rhyolitic material.

A peak in brown shards was isolated in direct association with the II-RHY-1 peak at 6 sites (Figure 4b; e.g. in MD99-2251 (Figure 4a)). Compositional analyses revealed a range of signatures with basaltic and intermediate material present (Figure 3aii). Shards related to three of the basaltic populations of Kvamme et al. (1989) have been identified, but no shards related to the II-THOL-3 population were isolated (Figure 3c). Glass shards with an intermediate trachyandesite to trachydacite composition have been identified (Figure 3aii) and grouped as a new population, which we name II-INT-1. Some material with an intermediate composition was found in association with the proximal Icelandic deposit correlated to NAAZ II, the Thorsmörk ignimbrite (Jørgensen, 1980), however, this is less evolved than the material in these marine deposits with SiO_2 values of 56-58 % and is unlikely to be directly related. This additional intermediate population suggests that the basaltic material associated with NAAZ II derives from more individual eruptions than previously thought. This assertion is also supported by differences in the composition of material from this study attributed to the populations of Kvamme et al. (1989) which may indicate they grouped material from multiple eruptions as single populations. For example, shards from M23485-1 and GIK23415-9 display geochemical differences, e.g. Figure 3cii, despite all falling into the II-THOL-2 field of Kvamme et al. (1989). At three of the sites the brown shards are related to a single population, homogenous populations within the II-THOL-2 geochemical field in M23485-1 and JM11-19PC and only shards from the intermediate population are present in MD01-2461 (Figure 4c). The remaining three sites preserve a mix of populations. MD04-2820CQ preserves three populations (II-THOL-1, II-THOL-2 and II-INT-1), each exceeding 24% of the shards present. GIK23415-9 and MD99-2251 are dominated by the II-THOL-1 and II-TAB-1 populations respectively.

The contrast between the homogeneity of the rhyolitic material at all sites and the heterogeneity and inconsistent signatures of the basaltic/intermediate material may indicate that despite coeval deposition the two components were transported differentially. It has been suggested that NAAZ II was primarily transported from Iceland via sea-ice rafting and primary airfall (e.g. Ruddiman and Glover, 1972; Austin et al., 2004; Wastegård et al., 2006). Sea-ice rafting may have contributed towards the relatively higher rhyolitic shard concentrations at sites to the south and west of Iceland. The geochemical homogeneity and distinct peak with an upward tail in rhyolitic shard concentrations (i.e. Type 3 deposits; e.g. Figure 4ai), observed at all sites is consistent with these transport processes and supports the isochronous nature of the II-RHY-1 component.

The heterogeneity of the basaltic material and relative discreteness of the concentration peaks, e.g. Figure 4aii, is most consistent with transport via iceberg rafting and the between-site contrasts in geochemical signatures highlights that icebergs calved from different margins of the Icelandic ice sheet could have transported and deposited material at the core sites. The absence of basaltic material associated with the rhyolitic peaks in the MD04-2822 and MD95-2010 sites is consistent with the findings of Abbott et al. (submitted) that ice rafting did not transport tephra to these sites during the last glacial period. Transportation via iceberg rafting can delay the deposition of tephra, therefore the peaks in basaltic material related to NAAZ II should not be utilised as isochronous markers. It cannot be ruled out that one or more of the basaltic populations were deposited coevally via primary airfall with the rhyolitic material, particularly at sites only containing one population. However, it is unlikely that this process deposited all of the basaltic populations with subsequent amalgamation in the sediment column, as shard concentrations profiles for that type of deposit (Type 4) typically have a greater spread within sequences and display multiple concentration peaks.

The coeval deposition of the two shard types may indicate that the volcanic eruption that produced the rhyolitic tephra horizon triggered an ice-rafting event which deposited the basaltic material, but the resolution of the marine records under investigation here is insufficient to resolve this temporal phasing.

4.1.2 FMAZ IV – MD95-2010 915-916 cm

FMAZ IV was identified in the MD95-2010 core from the Norwegian Sea as a discrete deposit at 915-916 cm depth (Figure 5a). This deposit has a homogenous basaltic composition with affinities to the Icelandic tholeiitic rock suite and the products of the Grímsvötn volcanic system. The composition of MD95-2010 915-916 cm is identical to the characterisation of the JM11-19PC 542-543 cm deposit of Griggs et al. (2014) (Figure 5b; SC – 0.985), previously correlated to the FMAZ IV of Wastegård and Rasmussen (2014). According to the age model and stratigraphy for MD95-2010 from Dokken and Jansen (1999) this layer has an age of ~44.45 ka BP and was deposited during the DO-12 event based on the magnetic susceptibility record. This stratigraphic position and age estimate are consistent with the work of Wastegård and Rasmussen (2014). This horizon has previously not been identified outside the Faroe Islands region and, therefore, this discovery expands its geographical range in a North easterly direction to the Nordic Sea.

4.1.3 MD04-2820CQ 524-525 cm

MD04-2820CQ 524-525 cm has previously been described by Abbott et al. (2016) where it was identified as a clear peak in shard concentrations spanning ~6 cm depth. Geochemical analyses of shards from this deposit form a homogenous tholeiitic basaltic population sourced from either the Grímsvötn or Kverkfjöll Icelandic volcanic systems. These characteristics allow the deposit to be defined as Type 2A and allied with a lack of direct covariance with IRD this deposit is thought to have been deposited via primary airfall despite occurring during a period of elevated IRD concentrations (Abbott et al., 2016).

4.1.4 MD04-2822 2017-2018 cm

High-resolution analysis of MD04-2822 showed a well-constrained peak in brown tephra shards in all grain-size fractions at 2017-2018 cm depth (Figure 6a). According to the core stratigraphy this horizon was deposited during a stadial period prior to the warming transition into DO-9 (Figure 6a). Shards have a homogenous basaltic composition with affinities to the Icelandic tholeiitic rock suite and the products of the Grímsvötn volcanic system (Figure 6c).

4.1.5 MD04-2820CQ 497-498 cm

MD04-2820CQ 497-498 cm was identified as a small peak in colourless shards during a period of consistently elevated concentrations (Abbott et al., 2016). Shards from the peak have a transitional alkali rhyolitic composition and form a single population with affinities to a number of distal tephra deposits previously attributed to the Katla volcanic system (Abbott et al., 2016). This horizon is notable as it is the only other rhyolitic horizon within the marine tephra framework apart from the rhyolitic component of NAAZ II (Table 1). Due to its homogeneity and the prevalence of shards in the 25-80 µm fraction this deposit was interpreted as an isochronous horizon deposited via primary airfall (Abbott et al., 2016).

4.1.6 MD04-2820CQ 487-488 cm

Deposited just prior to Heinrich Event 4, MD04-2820CQ 487-488 cm was identified as a clear peak in brown shard concentrations across all grain size fractions spread over ~3 cm depth (Abbott et al., 2016). While some transitional alkali outliers are present within shard analyses from this deposit the vast majority of shards (~85 %) form a homogenous geochemical population with a tholeiitic basaltic composition and affinities to the Grímsvötn volcanic system (Abbott et al., 2016). This homogenous composition and a lack of covariance of shard concentrations with IRD suggests it was not deposited via iceberg rafting. Deposition is likely to have occurred via primary airfall, however, the high proportion of shards in the coarser grain-size fractions (80-125 µm and >125 µm) in comparison to the 25-80 µm fraction may also indicate transport via sea-ice rafting. Neither process would impart a significant temporal delay and thus MD04-2820CQ 487-488 cm is viewed as an isochronous deposit (Abbott et al., 2016).

4.1.7 MD04-2829CQ 934-935 cm and 930-931 cm

Two distinct and closely spaced peaks in brown glass tephra shards were isolated in MD04-2829CQ with concentrations of ~35 shards per 0.5 g dws in the 25-80 µm grain-size fraction (Figure 6b). Only a limited number of shards were isolated in one of the three samples between these peaks. The stratigraphy for MD04-2829CQ indicates that these horizons were deposited during and just after the rapid warming into DO-8 (Figure 6b; Hall et al., 2011). Shards from both peaks were geochemically analysed and this revealed two homogenous basaltic populations with affinities to the Icelandic tholeiitic rock suite and the products of the Grímsvötn volcanic system. However, there are distinct differences in Al_2O_3, FeO, CaO and MgO between the two deposits (Figure 6c). These differences show that despite being separated by only 3 cm of sediment the horizons were produced by two separate volcanic eruptions and coupled with their other characteristics can be considered as valuable isochronous marker horizons.

4.1.8 MD04-2822 2004-2005 cm

High-resolution shard counts identified brown shards within the 25-80 and >125 µm grain-size fractions in the 2004-2005 cm sample of MD04-2822 (Figure 6a). While the shard concentrations are low the peaks are discrete as no further shards were identified in adjacent samples. According to the stratigraphy of the core this material was deposited shortly after the warming transition into DO-8 (Figure 6a; Hibbert et al., 2010). Geochemical analysis shows that shards from the deposit have a homogenous transitional alkali basaltic composition (Figure 6c). The shards are characterised by high TiO_2 values of ~4.65 %wt and comparisons to proximal Icelandic deposits demonstrate that the deposit was most likely sourced from the Katla volcanic system (Figure 6c). The geochemical composition of the material in this peak is very distinct from the material in the underlying MD04-2822 2017-2018 cm horizon indicating that they represent two discrete events.

4.1.9 MD99-2251 1680-1681 cm

The highest brown shard concentrations in MD99-2251 were identified as a peak centred around 1680-1681 cm depth (Figure 7a). Overall, high shard concentrations associated with this peak cover approximately 10 cm depth, typical of a Type 2 deposit, and glass shards from the main peak and a secondary peak at 1683-1684 cm were geochemically analysed.

Shards from 1680-1681 cm form a clear homogenous population, with 76 % of the analyses in this population (Figure 7b). High TiO_2 concentrations in excess of 4.4 %wt strongly indicates an origin from the Katla volcanic system (Figure 7b). Within the remaining 25 % of shards a minor population (6 %) of tholeiitic material, most likely sourced from the Kverkfjöll volcanic system, was also identified alongside several outlying shards (Figure 7b). The significant dominance of a single homogenous population in the 1680-1681 cm peak, suggests that this material was deposited via primary airfall and that this tephra deposit represents an isochronous marker horizon despite being deposited during a period of elevated IRD concentrations associated with Heinrich Event 3 (Figure 7a).

The geochemical signature of material from the underlying 1683-1684 cm peak is the same as the major 1680-1681 cm peak suggesting that this does not represent an earlier and separate depositional event but downward reworking of material from the main concentration peak. The slight deviation of the shard concentration profile from a gradational downward tail could imply that any reworking processes were not uniform across the core. Such variability was observed by Griggs et al. (2015) in 3D reconstructions of the structure of tephra deposits gained using X-ray microtomography.

4.1.10 MD04-2829CQ 800-801 cm

The highest shard concentrations in core MD04-2829CQ were identified at 800-801 cm, with increases observed in all grain-size fractions (Figure 6b). This deposit is very distinct with limited shards identified in adjacent samples. Stratigraphic constraints indicate that this horizon was deposited in the cold period prior to DO-4 (Figure 6b; Hall et al., 2011). Compositional analysis of individual shards shows that all material has a tholeiitic basaltic composition and can be grouped into two homogenous populations, with clear bimodality observed for some oxides, including TiO_2, FeO, CaO and MgO (Figure 6c). Analyses grouped into population THOL-1 were only derived from shards from the 25-80 µm grain-size fraction, whereas the majority of analyses in population THOL-2 are from shards >80 µm in diameter. Based on comparisons to proximal Icelandic deposits THOL-1 has a close affinity to products of Grímsvötn while THOL-2 is most likely derived from the Kverkfjöll volcanic system (Figure 6b). This implies that the deposit was formed from the deposition of material from two coeval eruptions of these volcanic centres.

4.1.11 MD04-2822 1836-1837 cm - GIK23415-9 225-226 cm

Within the MD04-2822 record the largest peak in brown shards was identified at 1836-1837 cm depth with >40 shards per 0.5 g of dws present in the 25-80 μm fraction (Figure 6a). The material is stratigraphically well constrained with only 2 shards present in the underlying sample. According to the stratigraphy this material was deposited during the cold stadial period shortly before the transition into DO-4 (Hibbert et al., 2010). Compositional analysis shows that material from this peak has a transitional alkali basaltic composition and forms a homogenous geochemical population (Figure 6c). Comparisons to proximal Icelandic deposits indicate that the horizon was sourced from either the Katla or Hekla/Vatnafjöll volcanic system (Figure 6c).

A discrete peak in shard concentrations, restricted to 1 cm and with the characteristics of a Type 1 deposit, was also isolated between 225-226 cm in GIK23415-9 (Figure 8a). Geochemical analysis of the shards from this deposit shows that all have a transitional alkali composition (Figure 8b). Within the analyses bimodality can be observed for some elements, most notably TiO_2, and they can be split into two homogenous populations. A dominant population (TAB-1) of 70 % of the shards with low TiO_2 values and a smaller population (TAB-2) of 15 % of the analysed shards with TiO_2 values ~0.35% wt higher. TiO_2 values have been identified as one of the primary oxides that can be used to discriminate between Icelandic basaltic eruptions from the last glacial period (e.g. Bourne et al., 2013, 2015). The remaining 15 % of analyses are classified as outliers. Comparisons to proximal deposits show that the populations have similarities to the products of both the Katla and Hekla/Vatnafjöll volcanic systems (Figure 8b). GIK23415-9 225-226 cm was deposited during Heinrich Event 3 which could suggest it was deposited via iceberg rafting. However, the relative dominance of the TAB-1 population and a lack of direct covariance of shard concentrations with IRD, with the discrete tephra peak contrasting with elevated IRD concentrations for ~25 cm of core depth, do not support this interpretation. These indicators provide support for primary airfall deposition of tephra shards from either a single chemically bimodal eruption or two closely timed events.

Statistical analysis (SC of 0.987) and graphical comparisons support a correlation between MD04-2822 1836-1837 cm and GIK23415-9 225-226 cm (TAB-1) (Table S13; Figure 9a). In addition, there is a consistency in the stratigraphic position of the two horizons. MD04-2822 1836-1837 cm was deposited between DO events 5 and 4 (Figure 6a), while GIK23415-9 225-226 cm was deposited at the end of Heinrich Event 3 (Figure 8a), which, based on a comparison of ages for the Heinrich Events from Sanchez Goñi and Harrison (2010) and the Greenland ice-core chronology presented in Seierstad et al. (2014), occurred after Greenland Interstadial (GI) 5, the ice counterpart to DO-5. Based on the available information, we assert that these two deposits are the products of the same volcanic event and form a tie-line between the two relatively closely spaced sequences (Figure 2).

4.1.12 GIK23415-9 173-174 cm

A peak in basaltic glass shard concentrations was identified in the GIK23415-9 core at a depth of 173-174 cm, following Heinrich Event 2 (Figure 8a). The shard concentration profile of this deposit is akin to a Type 1 deposit with a relatively discrete peak in shard concentrations restricted to ~1 cm (Figure 8a). Geochemical analysis of shards from this deposit show one clear homogenous population, composed of 60 % of the analysed shards, with a basaltic tholeiitic composition and an affinity to the Kverkfjöll volcanic system (Figure 8b). The remaining 40 % are heterogeneous and can be regarded as outliers (Figure S8). While the overall homogeneity of the deposit is not as distinct as most Type 1 deposits, the occurrence of a very homogenous population deposited during a period of low IRD input does suggest that airfall deposition occurred and it forms an isochronous deposit. The outlying shards may derive from a low background of IRD input of ice-rafted shards during this period. In addition, the use of the percentage abundance of populations to assess this deposit has some limitations as only a low number of analyses, 15, were gained from shards within this deposit.

4.2 Significant Geochemical Populations and Possible Isochrons

In addition to the isochronous deposits outlined in Section 4.1 six tephra deposits in the MD99-2251 core and four in the GIK23415-9 sequence were assessed as having non-isochronous characteristics and have been classified as Type 2B or Type 4 deposits (Figures 7a and 8a). The main criterion underpinning this assessment was the geochemical heterogeneity of the deposits, indicative of the amalgamation of material from a number of volcanic eruptions. However, while only three deposits, MD99-2251 1654-1655 cm and

1796-1797 cm and GIK23415-9 193-194 cm, have fully heterogenous compositions the other deposits contain 16 significant homogenous geochemical populations, in total, within their overall heterogeneity (Figure 2; Table 1). The significant geochemical populations may relate to single volcanic eruptions, but due to their occurrence within heterogenous deposits further investigations are required to determine if they were deposited isochronously. The full geochemical signatures of all MD99-2251 and GIK23415-9 deposits and the populations identified within them are summarised in Figures S1-S14 and Tables S8 and S10.

The 16 populations all have a basaltic composition and were sourced from Iceland. In addition to the volcanic regions which deposited isochronous horizons in the North Atlantic region, i.e. Grímsvötn, Kverkfjöll, Hekla/Vatnafjöll and Katla, homogenous populations with geochemical similarities to the products of the Veidivötn-Bardarbunga and Vestmannaeyjar volcanic systems were identified (Table 1; Figures 7a and 7b). Their relative dominance within the deposits is variable, ranging from ~10 to 60 % of the total single-shard analyses used to characterise the deposits (Tables S8 and S10).

Co-variance of shard concentration profiles with IRD records was another variable used to assess the isochronous nature of the deposits (Abbott et al., submitted). Some of the deposits with heterogenous signatures were deposited during periods of elevated or rising IRD concentration, which could indicate transport via iceberg rafting and a significant temporal delay between eruption and deposition. However, iceberg rafting is not the only process that can amalgamate the products of multiple eruptions. For example, for some deposits post-depositional mixing in the sediment column of the products of several closely-timed eruptions cannot be ruled out as some were isolated within periods of limited IRD deposition. In this later scenario deposition would have been via primary airfall with no temporal delay, however, determining the isochron position could be challenging as complexity is often observed in the shard concentration profiles. Primary airfall deposition could also have occurred during a period of ice-rafting deposition resulting in the incorporation of a homogenous population within a heterogenous background signal.

These differing scenarios and the uncertainty in the depositional processes implies that further investigations are required to assess whether these populations are isochronous. As such, we report the significant geochemical populations, but do not incorporate them within the regional tephra framework until further evidence is gained. The latter may include their identification in other North Atlantic marine cores and/or the Greenland ice-core tephra framework in a similar stratigraphic position. In addition, for some records the covariance with IRD could not be fully explored due to the lower resolution in this dataset relative to the shard concentration profiles. Improved high-resolution IRD records would be highly advantageous for further assessing depositional processes. An example of how tracing these populations into other records could provide further insights into their isochronous nature is provided within our work.

The assessment of potential correlations (Table S13), highlighted a strong similarity between the geochemical signature of FMAZ II and the THOL-1 population in the GIK23415-9 202-203 cm deposit (Figure 7; Table 1). The SC comparison returned a high coefficient of 0.990, demonstrating that the signatures were nearly identical, and this observation is corroborated by graphical comparisons (Figure 9b). Stratigraphically, FMAZ II has been identified between Heinrich Events 3 and 2 in marine records and was deposited prior to an increase in IRD concentrations in the ENAM93-21 core (Rasmussen et al., 2003) and after GI-3 in the Greenland ice-core stratigraphy (Davies et al., 2010). GIK23415-9 202-203 cm was deposited during a period of increasing IRD concentrations related to the start of Heinrich Event 2 (Figure 8a). These stratigraphic positions are consistent and coupled with the strong geochemical similarities could imply isochronous deposition from the same volcanic event. GIK23415-9 202-203 cm (THOL-1) is one of 4 homogenous geochemical populations within the deposit and, due to their co-occurrence, it was interpreted as being deposited via iceberg rafting. The proposed correlation does not contradict this interpretation but could demonstrate that GIK23415-9 202-203 cm (THOL-1) was deposited via airfall during a period when tephra from other events was rafted by icebergs. Overall, this further highlights the complexity of some deposits, but demonstrates how these significant geochemical populations are important to consider as potential isochronous markers.

5. Discussion

5.1 Future application of the North Atlantic Marine Tephra Framework

The North Atlantic marine tephra framework between MIS 2-3 has been significantly improved through the most extensive application of cryptotephra methods, comprehensive compositional analysis and rigorous protocols to assess the isochronous nature of each deposit. For a long period only a limited number of horizons had been identified in this time period (Haflidason et al., 2000; Wastegård et al., 2006). Now this framework includes 14 isochronous horizons that have considerable promise for correlating and synchronising palaeoclimatic records. There is also potential to add further isochronous markers given the significant geochemical populations identified in heterogenous deposits also reported in this study.

NAAZ II remains a dominant tephra within this framework and our work has identified it in numerous additional cores with greater control on the timing of deposition derived from high-resolution shard counts and an improved geochemical signature for the widespread rhyolitic component (II-RHY-1). This tephra represents a key marker horizon for the period providing an isochronous tie-line linking numerous widespread marine cores and the Greenland ice-core records beyond the radiocarbon window. The distribution of the FMAZ IV has been extended from the Faroe Islands region into the Nordic Seas and has the potential to be a key tie-line for DO 12. However, despite being found previously in several North Atlantic cores and the NGRIP ice-core (see summary map in Davies et al., 2012) the FMAZ II was only found in one additional core, GIK23415-9. Furthermore, most of the new cryptotephras are single-core occurrences, highlighting challenges with cryptotephra tracing within the North Atlantic Ocean. The limited tracing of horizons may reflect the difficulties of detecting and isolating deposits that often only contain a low concentration of shards, but could also indicate the relatively constrained dispersal of the basaltic eruptions depositing material over the North Atlantic. Only one correlation has been made between newly identified isochronous horizons in the framework, MD04-2822 1836-1837 cm and GIK23415-9 225-226 cm (Section 4.1.11; Figure 2). These cores are relatively closely spaced, supporting the suggestion of limited basaltic ash dispersal.

Assessing potential correlations between the records highlighted that while a range of factors demonstrated that there are few direct correlations, many of the horizons have similar geochemical signatures, especially eruptions from the Grímsvötn and Katla volcanic systems (Table 1). This corroborates the findings of Bourne et al. (2015) who observed similar repetition of geochemical signatures from these systems in tephra horizons in the Greenland ice-cores. The repetition of geochemical signatures is particularly notable for the period around H4 as a cluster of six closely spaced horizons has been identified in the marine cores (Figure 2). Of these, five horizons have similar tholeiitic basaltic compositions and are thought to be derived from the Grímsvötn volcanic system, however, subtle differences in geochemical signatures show they represent individual events.

The observations that the new cryptotephras in the North Atlantic region may have limited dispersal and geochemical similarities do provide challenges for future correlation. There is, however, the potential to constraint a number of rapid climate events, such as H4 and DO 8 and H3 as clusters of isochronous horizons are present around those events. Further investigations should initially focus on sites close to those preserving the isochronous horizons in this framework and/or re-evaluate previously explored sites (e.g. green sites on Figure 1), with adaptions to the methodological approach discussed in Section 5.3. It is imperative that potential correlations are rigorously assessed as correlating horizons or populations with close, but not identical, geochemical signatures, could lead to the establishment of incorrect tie-lines being defined between records. Other supporting evidence such as broad stratigraphic constraints and independent age estimates can also be used to support these correlations. A detailed assessment of possible correlations to the Greenland ice-cores will be discussed in a forthcoming publication whereby trace element signatures are also employed to assess and support correlations.

5.2 Reconstructing Icelandic Volcanic History

This framework adds to our understanding of the volcanic history of Iceland during the last glacial period between 25-60 kyr BP. The dominance of basaltic over rhyolitic horizons and the high productivity of the Grímsvötn/Kverkfjöll and Katla volcanic systems around Heinrich Event 4 and Henrich Event 3 respectively, is consistent with the Greenland ice-core tephra framework for the same period (Bourne et al., 2015). Basaltic horizons potentially sourced from other volcanic centres were observed, including the Veidivötn-Bardabunga and Vestmannaeyjar volcanic systems. There are very few or no tephras in the Greenland framework with geochemical similarities to those horizons, potentially due to a bias in dispersal direction and/or a low number of eruptions from these sources. This observation shows that a more complete reconstruction of Icelandic volcanism will be gained by integrating the two frameworks. There is, however, a notable difference between the number of tephra deposits identified between the marine and ice-core records. With 99 volcanic events recorded in the Greenland records in contrast to 33 events in the marine archives, if the homogenous populations are assumed to derive from individual volcanic events. The lower resolution of the marine records, the potential for the amalgamation of airfall deposits and post-depositional reworking processes are the most likely causes of this disparity.

5.3 Improving the Marine Tephra Framework

This work has demonstrated the potential of identifying isochronous cryptotephras in North Atlantic marine records of the last glacial period. However, the methodology employed to identify cryptotephras in this work most likely created a bias towards the identification of horizons depositing a high concentration of tephra shards at core sites. As discussed by Timms et al. (2017) the process of completing low-resolution scans prior to a subjective peak selection for high-resolution (1 cm) analysis may introduce a bias as low concentration or discrete peaks might not have sufficient shard concentrations to be observed in the low-resolution record. The background of tephra that is prevalent at some marine sites could mask individual eruptions that deposited a low concentration of shards. In the ice-core records tephra events have been defined on the basis of as few as 3 shards (Bourne et al., 2015). Detecting deposits of this kind would be particularly challenging in the marine environment as they could be dismissed as "background" concentrations or hidden with the upward or downward tail of a deposit or within an ash-rich deposit. We have attempted to explore the presence of such horizons in this study but agree with Timms et al. (2017) who advocate the use of more high-resolution shard concentration and chemical analyses to improve tephrostratigraphies, while acknowledging that this may be limited by sediment availability, time and financial considerations.

As such, the marine tephra framework presented in this study should not be viewed as complete. However, by focusing on maximising the number and geographical range of sequences an initial framework has been produced that is a significant step towards the tephra-based synchronisation of North Atlantic marine records. Coupling the success of the methodology, the initial framework presented here and the insights into the spatial controls on tephra deposition discussed in Abbott et al. (submitted) there is huge potential to add to and refine the marine tephra framework. This can be achieved through focusing on new cores from areas with a high potential to preserve isochronous horizons and reassessing previously investigated cores at a high-resolution over key intervals during which isochronous horizons were identified in this work. In addition, innovative techniques for the identification and quantification of tephra that are currently being developed, for example X-ray florescence core scanning (e.g. Kolling and Bauch, 2017), hyperspectral core imaging (e.g. Aymerich et al., 2016) and automated flow cytometry and microscopy (e.g. D'Anjou et al., 2014), could be tested and incorporated into the methodological approach if appropriate.

6. Conclusions

A consistent methodology for the identification and characterisation of marine cryptotephras and the rigorous assessment of the influence of transportation and deposition processes on tephra deposits was used to build a North Atlantic marine tephra framework. Eleven isochronous deposits were identified in a wide network of marine sequences and have been integrated with prior data to create a marine tephra framework for the MIS 2-3 period. Key information for each deposit such as their spatial extent, geochemical signature, eruptive source and timing of deposition is synthesised. A number of significant geochemical populations are also reported that require further work to assess whether they originate from single volcanic eruptions and were deposited isochronously via primary airfall.

There is considerable potential to improve this framework by tracing the deposits into other marine sequences or the identification of new deposits. Combining this framework with knowledge of the processes controlling the deposition of tephra in the North Atlantic and the identification of key areas where isochronous horizons are preserved provided in Abbott et al. (submitted) these future investigations could be highly focussed, both temporally and spatially. The full potential of this framework will only be realised if attempts are made to trace these horizons into other archives such as the Greenland ice-cores and terrestrial records. If successful they can act as time-synchronous tie-lines to correlate and synchronise these palaeoclimatic records, providing insights into the phasing, rate, timing and mechanisms forcing the rapid climate changes that characterised this period.

Acknowledgements

This work was financially supported by the European Research Council (TRACE project) under the European Union's Seventh Framework Programme (FP7/2007-2013) / ERC grant agreement no. [259253]. PMA also acknowledges support from the European Research Council under the European Union's Horizon 2020 research and innovation programme (grant agreement No 656381). Thanks to William Austin, Henning Bauch, Frederique

Eynaud, Ian Hall, Claude Hillaire-Marcel, Elisabeth Michel, Tine Rasmussen, Bjørg Risebrobakken, James Scourse, Mara Weinelt and the British Ocean Sediment Core Research Facility (BOSCORF) for providing samples or access to the marine cores utilised within this study. We would like to thank Dr Chris Hayward for his assistance with the use of the electron microprobe at the Tephrochronology Analytical Unit, University of Edinburgh. Thanks also to Gareth James, Gwydion Jones and Kathryn Lacey (Swansea University) for assistance with laboratory processing. This paper contributes to the EXTRAS project (EXTending TephRAS as a global geoscientific research tool stratigraphically, spatially, analytical, and temporally within the Quaternary), an INTAV-led project (International Focus Group on Tephrochronology and Volcanism) within the Stratigraphy and Chronology Commission (SACCOM) of the International Union for Quaternary research (INQUA).

Figures

Figure 1: Location map of cores within the marine network (red) and other cores referred to in the text (green). Location (1) includes cores SO82-2, SO82-5, LO09-23, LO09-21, SO82-7 and SO82-4 described in Lackschewitz and Wallrabe-Adams (1997). Location (2) includes cores ENAM93-21 and ENAM93-20 and location (3) includes cores LINK16, LINK17, LINK15 and LINK04 described in Rasmussen et al. (2003), Wastegård et al. (2006) and Wastegård and Rasmussen (2014).

Figure 2: Schematic representation of the improved marine tephra framework for the North Atlantic between 25-60 kyr BP. Ages and the stratigraphic relationship of tephra horizons between cores are approximate should be treated with caution, see text for details. The ages utilised are based on either existing age models for sequences or estimates based on stratigraphic positions. Heinrich Events 2-5 are included as stratigraphic markers and their ages are based on those given in Sanchez Goñi and Harrison (2010).

Figure 3: (a) Total alkali v silica plot focusing on (i) rhyolitic material and (ii) basaltic and intermediate composition material from NAAZ II deposits in the marine network. (b) Comparison of new characterisations of NAAZ II rhyolitic material to characterisations from prior studies. Geochemical fields based on deposits in cores V23-23, V27-114, V23-82, V23-81 and V23-42 (Kvamme et al., 1989), MD95-2006 (Austin et al., 2004), ENAM93-20, ENAM33 and EW9302-2JPC (Wastegård et al., 2006) and MD99-2289 (Brendryen et al., 2011). (c) Comparison of basaltic material from newly characterised NAAZ II deposits to basaltic NAAZ II populations defined by Kvamme et al. (1989).

Figure 4: (a) Tephrostratigraphy of MD99-2251 between 1950-2030 cm covering the depth interval of NAAZ II. (i) Rhyolitic shards in the 25-80 µm grain-size fraction. (ii) Basaltic shards in the 25-80 µm grain-size fraction. (b) Peak concentrations of colourless (rhyolitic) and brown (basaltic) glass tephra shards in tephra deposits related to North Atlantic Ash Zone II. (c) Relative proportion of geochemical populations within analyses of basaltic glass tephra shards from NAAZ II deposits at six sites within the marine core network. Shard analyses not linked to the previously published populations or II-INT-1 were classified as uncorrelated.

Figure 5: (a) High-resolution concentration profiles of brown glass tephra shards between 910-920 cm in MD95-2010. (b) Comparison of the composition of MD95-2010 915-916 cm to the characterisation of FMAZ IV (JM11-19PC 542-543 cm) from Griggs et al. (2014).

Figure 6: (a) (i) Percentage abundance of *Neogloboquadrina pachyderma* (sinistral) and (ii) brown glass tephra shard tephrostratigraphy incorporating 5 cm and 1 cm counts for the MD04-2822 core. (b) (i) Percentage abundance of *Neogloboquadrina pachyderma* (sinistral) and (ii) brown glass tephra shard tephrostratigraphy incorporating 5 cm and 1 cm counts for the MD04-2829CQ core. Foram abundances and Dansgaard-Oeschger event numbering for MD04-2822 and MD04-2829CQ from Hibbert et al. (2010) and Hall et al. (2011) respectively. (c) Geochemical characterisations of Type 1 tephra deposits in the MD04-2822 and MD04-2829CQ cores. (i) inset of total alkali vs. silica plot. Division line to separate alkaline and sub-alkaline material from MacDonald and Katsura (1964). Chemical classification and nomenclature after Le Maitre et al. (1989). (ii) FeO/TiO_2 vs. SiO_2 and (iii) TiO_2 vs. Al_2O_3 compositional variations diagrams comparing the composition of MD04-2822 and MD04-2829CQ deposits to characterisations of proximal Icelandic material. Geochemical fields for Icelandic source volcanoes are based on those utilised in Bourne et al. (2015) and references within.

Figure 7: (a) (i) Percentage abundance of *Neogloboquadrina pachyderma* (sinistral), (ii) ash free IRD concentration and (iii) tephrostratigraphic record of the MD99-2251 marine core. Shard counts have been truncated for clarity. Shard counts in the 1686-1687 cm sample (*) are 4991, 1862 and 507 shards per 0.5 g dws in the 25-80, 80-125 and >125 µm grain-size fractions respectively. The shard counts for the 25-80 µm grain-size fraction from the 1904-1905 cm sample (**) are 3776 shards per 0.5 g dws. Red bars denote samples depths from which glass shards were subsequently extracted for compositional characterisation. (b) Composition of significant geochemical populations identified in tephra deposits within the MD99-2251 core. (i) inset of total alkali vs. silica plot. Division line to separate alkaline and sub-alkaline material from MacDonald and Katsura (1964). Chemical classification and nomenclature after Le Maitre et al. (1989). (ii) FeO/TiO_2 vs. SiO_2 and (iii) TiO_2 vs. Al_2O_3 compositional variations diagrams comparing significant geochemical populations from the MD99-2251 deposits to characterisations of proximal Icelandic material. Geochemical fields for Icelandic source volcanoes are based on those utilised in Bourne et al. (2015) and references within.

Figure 8: (a) (i) Percentage abundance of *Neogloboquadrina pachyderma* (sinistral), (ii) percentage IRD (>150 µm fraction) and (iii) tephrostratigraphic record of the GIK23415-9 marine core. *Np*(s) and IRD data from Vogelsang et al. (2004) and Weinelt (2004) respectively. Labels for Heinrich Events from Weinelt et al. (2003) and Lu et al. (2007). Shard counts have been truncated for clarity. Shard counts in the 193-194 cm sample are 5131 and 280 shards per 0.5 g dws in the 25-80 and >125 µm grain-size fractions respectively. Red bars denote samples depths from which glass shards were subsequently extracted for compositional characterisation. (b) Composition of significant geochemical populations identified in tephra deposits within the GIK23415-9 core. (i) inset of total alkali vs. silica plot. Division line to separate alkaline and sub-alkaline material from MacDonald and Katsura (1964). Chemical classification and nomenclature after Le Maitre et al. (1989). (ii) FeO/TiO_2 vs. SiO_2 and (iii) TiO_2 vs. Al_2O_3 compositional variations diagrams comparing significant geochemical populations from the GIK23415-9 deposits to characterisations of proximal Icelandic material. Geochemical fields for Icelandic source volcanoes are based on those utilised in Bourne et al. (2015) and references within.

Figure 9: (a) Comparison of the MD04-2822 1836-1837 cm tephra horizon and the GIK23415-9 225-226 cm (TAB-2) geochemical population. (b) Comparison of the FMAZ II tephra horizon (JM11-19PC 202-203 cm from Griggs et al. (2014)) and the GIK23415-9 202-203 cm (THOL-1) geochemical population.

Supplementary Information

Supplementary Figures

Figures S1-S13: Graphical analysis of geochemical populations identified within single-shard major element analyses from tephra deposits within the MD99-2251 (S1-S7) and GIK23415-9 (S8-S13) cores.

Supplementary Data

Table S1: Major oxide concentrations of shards from deposits related to the rhyolitic component of North Atlantic Ash Zone II (II-RHY-1). Deposits analysed are (i) MD04-2822 2168-2169 cm (ii) MD95-2024 1445-1446 cm (iii) MD99-2251 1974-1975 cm (supplementary peak) (iv) MD99-2251 2014-2015 cm (main peak) (v) M23485-1 622-623 cm (vi) GIK23415-9 429-430 cm (vii) MD01-2461 942-943 cm (supplementary peak) (viii) MD01-2461 947-948 cm (main peak) (ix) MD04-2820CQ 610-611 cm (x) JM11-19PC 618-623 cm (xi) MD95-2010 996-1000 cm.

Table S2: Similarity coefficient comparisons of average concentrations of analyses of the II-RHY-1 component in deposits from cores analysed within this work and by Kvamme et al. (1989), Austin et al. (2004), Wastegård et al. (2006) and Brendryen et al. (2011).

Table S3: Major oxide concentrations of shards from basaltic and intermediate shards directly associated with deposits of the rhyolitic component of North Atlantic Ash Zone II (II-RHY-1). Deposits analysed are (i) MD99-2251 2014-2015 cm (ii) M23485-1 622-623 cm (iii) GIK23415-9 429-430 cm (iv) MD01-2461 947-948 cm (v) MD04-2820CQ 610-611 cm (vi) JM11-19PC 618-623 cm.

Table S4: Major oxide concentrations of shards from the MD95-2010 915-916 cm tephra deposit.

Table S5: Major oxide concentrations of shards from tephra deposits in the MD04-2822 core. Deposits analysed are from the depths of (i) 1836-1837 cm (ii) 2004-2005 cm and (iii) 2017-2018 cm.

Table S6: Major oxide concentrations of shards from tephra deposits in the MD04-2829CQ core. Deposits analysed are from the depths of (i) 800-801 cm (ii) 930-931 cm and (iii) 934-935 cm.

Table S7: Major oxide concentrations of shards from tephra deposits in the MD04-2820CQ core. Deposits analysed are from the depths of (i) 487-488 cm (ii) 497-498 cm and (iii) 524-525 cm.

Table S8: Major oxide concentrations of shards from tephra deposits in the MD99-2251 core. Deposits analysed are from the depths of (i) 1654-1655 cm (ii) 1680-1681 cm (iii) 1683-1684 cm (iv) 1713-1714 cm (v) 1772-1773 cm (vi) 1796-1797 cm (vii) 1812-1813 cm and (viii) 1904-1905 cm.

Table S9: Analysis of geochemical populations present within tephra deposits identified in the MD99-2251 marine core. n = total number of analyses from deposits. Veid.-Bárd. = Veidivötn-Bárdarbunga.

Table S10: Major oxide concentrations of shards from tephra deposits in the GIK23415-9 core. Deposits analysed are from the depths of (i) 173-174 cm (ii) 193-194 cm (iii) 202-203 cm (iv) 225-226 cm (v) 302-303 cm (vi) 305-306 cm and (vii) 375-376 cm.

Table S11: Analysis of geochemical populations present within tephra deposits identified in the GIK23415-9 marine core. n = total number of analyses from deposits. Veid.-Bárd. = Veidivötn-Bárdarbunga.

Table S12a: Secondary standard analyses of the BCR2g standard made throughout analytical periods during which sample analyses presented in this work were analysed.

Table S12b: Secondary standard analyses of the Lipari standard made throughout analytical periods during which sample analyses presented in this work were analysed.

Table S13: Similarity coefficient comparisons between the geochemical signatures of isochronous horizons and significant geochemical populations in the marine tephra framework for the North Atlantic between 25-60 ka BP. Method of Borchardt et al. (1972) utilised. Red text shows SC values between 0.97 and 0.999 grey text shows SC values less than 0.95.

References

Abbott, P.M., Bourne, A.J., Purcell, C.S., Davies, S.M., Scourse, J.D., Pearce, N.J.G., 2016. Last Glacial Period Cryptotephra Events in an Eastern North Atlantic Ocean Marine Sequence: Exploring Linkages to the Greenland Ice-Cores. Quaternary Geochronology 31, 62-76.

Abbott, P.M., Austin, W.E.N., Davies, S.M., Pearce, N.J.G., Hibbert, F.D., 2013. Cryptotephrochronology of a North East Atlantic marine sequence over Termination II, the Eemian and the last interglacial-glacial transition. Journal of Quaternary Science 28, 501-514.

Abbott, P.M., Austin, W.E.N., Davies, S.M., Pearce, N.J.G., Rasmussen, T.L., Wastegård, S., Brendryen, J., 2014. Re-evaluation and extension of the MIS 5 tephrostratigraphy of the Faroe Islands Region: the cryptotephras record. Palaeogeography, Palaeoclimatology, Palaeoecology 409, 153-168.

Abbott, P.M., Davies, S.M., 2012. Volcanism and the Greenland ice-cores: the tephra record. Earth-Science Reviews 115, 173-191.

Abbott, P.M., Davies, S.M., Austin, W.E.N., Pearce, N.J.G., Hibbert, F.D., 2011. Identification of cryptotephra horizons in a North East Atlantic marine record spanning marine isotope stages 4 and 5a (~60,000-82,000 a b2k). Quaternary International 246, 177-189.

Abbott, P.M., Griggs, A.J., Bourne, A.J., Davies, S.M., submitted. Tracing marine cryptotephras in the North Atlantic during the Last Glacial Period: Identification, characterisation and depositional controls. Submitted to Quaternary Science Reviews.

Austin, W.E.N., Abbott, P.M., 2010. Comment: Were last glacial climate events simultaneous between Greenland and France? A quantitative comparison using non-tuned chronologies. M. Blaauw, B. Wohlfarth, J.A. Christen, L. Ampel, D. Veres, K. Hughen, F. Preusser and A. Svensson (2009). Journal of Quaternary Science 25, 1045-1046.

Austin W.E.N., Wilson L.J., Hunt J.B., 2004. The age and chronostratigraphical significance of North Atlantic Ash Zone II. Journal of Quaternary Science 19, 137-146.

Aymerich, I.F., Oliva, M., Giralt, S., Martin-Herrero, 2016. Detection of Tephra Layers in Antarctic Sediment cores with Hyperspectral Imaging. PLoS ONE 11(1): e0146578. doi:10.1371/ journal.pone.0146578.

Blockley, S.P.E., Bourne, A.J., Brauer, A., Davies, S.M., Hardiman, M., Harding, P.R., Lane, C.S., MacLeod, A., Matthews, I.P., Pyne-O'Donnell, S.D.F., Rasmussen, S.O., Wulf, S., Zanchetta, G., 2014. Tephrochronology and the extended intimate (integration of ice-core, marine and terrestrial records) event stratigraphy 8-128 ka b2k. Quaternary Science Reviews 106, 88-100.

Bond, G., Broecker, W., Johnsen, S., McManus, J., Labeyrie, L., Jouzel, J., Bonani, G., 1993. Correlations between climate records from North Atlantic sediments and Greenland ice. Nature 365, 143-147.

Borchardt, G.A., Aruscavage, P.J., Millard, H., 1972. Correlation of the Bishop ash, a Pleistocene marker bed, using instrumental neutron activation analysis. Journal of Sedimentary Petrology 42, 201-206.

Bourne, A.J., Davies, S.M., Abbott, P.M., Rasmussen, S.O., Steffensen, J.P., Svensson, A., 2013. Revisiting the Faroe Marine Ash Zone III in two Greenland ice cores: implications for marine-ice correlations. Journal of Quaternary Science 28, 641-646.

Bourne, A.J., Cook, E., Abbott, P.M., Seierstad, I.K., Steffensen, J.P., Svensson, A., Fischer, H., Schupbach, S., Davies, S.M., 2015. A tephra lattice for Greenland and a reconstruction of volcanic events spanning 25-45 ka b2k. Quaternary Science Reviews 118, 122-141.

Bramlette M.N., Bradley W.H., 1941. Geology and biology of North Atlantic deep-sea cores between Newfoundland and Ireland: I. Lithology and geologic interpretation. U.S. Geological Survey Professional Paper 196-A, 1-34.

Brendryen, J., Haflidason, H., Sejrup, H.P., 2010. Norwegian Sea tephrostratigraphy of marine isotope stages 4 and 5: Prospects and problems for tephrochronology in the North Atlantic region. Quaternary Science Reviews 29, 847-864.

Brendryen, J., Haflidason, H., Sejrup, H.P., 2011. Non-synchronous deposition of North Atlantic Ash Zone II in Greenland ice cores, and North Atlantic and Norwegian Sea sediments: an example of complex glacial-stage tephra transport. Journal of Quaternary Science 26, 739-745.

D'Anjou, R.M., Balascio, N.L., Bradley, R.S., 2014. Locating cryptotephra in lake sediments using fluid imaging technology. Journal of Paleolimnology 52, 257-264.

Davies, S.M., 2015. Cryptotephras: the revolution in correlation and precision dating. Journal of Quaternary Science 30, 114-130.

Davies, S.M., Abbott, P.M., Meara, Rh. H., Pearce, N.J.G., Austin, W.E.N., Chapman, M. R., Svensson, A., Bigler, M., Rasmussen, T.L., Rasmussen, S.O., Farmer, E.J., 2014. A North Atlantic tephrostratigraphical framework for 130-60 ka b2k: new tephra discoveries, marine-based correlations, and future challenges. Quaternary Science Reviews 106, 101-121.

Davies, S.M., Abbott, P.M., Pearce, N.J.G., Wastegård, S., Blockley, S.P.E., 2012. Integrating the INTIMATE records using tephrochronology: rising to the challenge. Quaternary Science Reviews 36, 11-27.

Davies, S.M., Wastegård, S., Abbott, P.M., Barbante, C., Bigler, M., Johnsen, S.J., Rasmussen, T.L., Steffensen, J.P., Svensson, A., 2010. Tracing volcanic events in the NGRIP ice-core and synchronising North Atlantic marine records during the last glacial period. Earth and Planetary Science Letters 294, 69-79.

Davies, S.M., Wastegård, S., Rasmussen, T.L., Svensson, A., Johnsen, S.J., Steffensen, J.P., Andersen, K.K., 2008. Identification of the Fugloyarbanki tephra in the NGRIP ice core: a key tie-point for marine and ice-core sequences during the last glacial period. Journal of Quaternary Science 23, 409-414.

Dokken, T.M., Jansen, E., 1999. Rapid changes in the mechanism of ocean convection during the last glacial period. Nature 401, 458-461.

Griggs, A.J., Davies, S.M., Abbott, P.M., Coleman, M., Palmer, A.P., Rasmussen, T.L., Johnston, R., 2015. Visualising tephra sedimentation processes in the marine environment: the potential of X-ray microtomography. Geochemistry, Geophysics, Geosystems 16, doi: 10.1002/2015GC006073.

Griggs, A.J., Davies, S.M., Abbott, P.M., Rasmussen, T.L., Palmer, A.P., 2014. Optimising the use of marine tephrochronology in the North Atlantic: A detailed investigation of the Faroe Marine Ash Zones II, III and IV. Quaternary Science Reviews 106, 122-139.

Grönvold K., Óskarsson N., Johnsen S.J., Clausen H.B., Hammer C.U., Bond G., Bard E., 1995. Ash layers from Iceland in the Greenland GRIP ice core correlated with oceanic and land sediments. Earth and Planetary Science Letters 135, 149-155.

Gudmundsdóttir, E.R., Larsen, G., Björck, S., Ingólfsson, Ó., Striberger, J., 2016. A new high-resolution tephra stratigraphy in eastern Iceland: Improving the Icelandic and North Atlantic tephrochronology. Quaternary Science Reviews 150, 234-249.

Haflidason H., Eiriksson J., Van Kreveld S., 2000. The tephrochronology of Iceland and the North Atlantic region during the Middle and Late Quaternary: a review. Journal of Quaternary Science 15, 3-22.

Hall, I.R., Colmenero-Hidalgo, E., Zahn, R., Peck, V.L., Hemming, S.R., 2011. Centennial- to millennial-scale ice-ocean interactions in the subpolar northeast Atlantic 18-41 kyr ago. Paleoceanography 26, PA2224, doi:10.1029/2010PA002084.

Henry, L.G., McManus, J.F., Curry, W.B., Roberts, N.L., Piotrowski, A.M., Keigwin, L.D., 2016. North Atlantic ocean circulation and abrupt climate change during the last glaciation. Science 353, 470-474.

Hibbert, F.D., Austin, W.E.N., Leng, M.J., Gatliff, R.W., 2010. British Ice Sheet dynamics inferred from North Atlantic ice-rafted debris records spanning the last 175 000 years. Journal of Quaternary Science 25, 461-482.

Hunt, J.B., Hill, P.G., 2001. Tephrological implications of beam size-sample-size effects in electron microprobe analysis of glass shards. Journal of Quaternary Science 16, 105-117.

Jørgensen, K.A., 1980. The Thorsmork ignimbrite: An unusual comenditic pyroclastic flow in Southern Iceland. Journal of Volcanology and Geothermal Research 8, 7-22.

Kolling, H., Bauch, H. A., 2017. A Stratigraphical-Sedimentological Study of the Last Interglacial Period in the Central Nordic Seas on the Basis of XRF Core Scanning. Polarforschung 87, 15-22.

Kuehn, S.C., Froese, D.G., Shane, P.A.R., INTAV Intercomparison Participants (2011) "The INTAV intercomparison of electron-beam microanalysis of glass by tephrochronology laboratories: Results and recommendations", *Quaternary International* **246**, 19-47.

Kvamme T, Mangerud J, Furnes H, Ruddiman W. 1989. Geochemistry of Pleistocene ash zones in cores from the North Atlantic. *Norsk Geologisk Tidskrift* **69**: 251-272.

Lacasse C, Sigurdsson H, Carey S, Paterne M, Guichard F. 1996. North Atlantic deep-sea sedimentation of Late Quaternary tephra from the Iceland hotspot. *Marine Geology* **129**: 207-235.

Lackschewitz, K.S., Wallrabe-Adams, H.-J., 1997. Composition and origin of volcanic ash zones in Late Quaternary sediments from the Rekjanes Ridge: evidence for ash fallout and ice-rafting. Marine Geology 136, 209-224.

Lane, C.S., Brauer, A., Blockley, S.P.E., Dulski, P., 2013. Volcanic ash reveals time-transgressive abrupt climate change during the Younger Dryas. Geology 41, 1251-1254.

Le Maitre, R.W., Bateman, P., Dudek, A., Keller, J., Lameyre, Le Bas, M.J., Sabine, P.A., Schmid, R., Sorensen, H., Streckeisen, A., Woolley, A.R., Zanettin, B., 1989. A Classification of Igneous Rocks and Glossary of Terms. Blackwell, Oxford.

Lowe, D.J., 2011. Tephrochronology and its application: A review. Quaternary Geochronology 6, 107-153.

Lowe, D.J., Shane, P.A.R., Alloway, B.V., Newnham, R.M., 2008. Fingerprints and age models for widespread New Zealand tephra marker beds erupted since 30,000 years ago: a framework for NZ-INTIMATE. Quaternary Science Reviews 27, 95-126.

Lowe, J.J., Barton, N., Blockley, S., Bronk Ramsey, C., Cullen, V.L., Davies, W., Gamble, C., Grant, K., Hardiman, M., Housley, R., Lane, C.S., Lee, S., Lewis, M., MacLeod, A., Menzies, M., Müller, W., Pollard, M., Price, C., Roberts, A.P., Rohling, E.J., Satow, C., Smith, V.C., Stringer, C.B., Tomlinson, E.L., White, D., Albert, P., Arienzo, I., Barker, G., Borić, D., Carandente, A., Civetta, L., Ferrier, C., Guadelli, J.-L., Karkanas, P., Koumouzelis, M., Müller, U.C., Orsi, G., Pross, J., Rosi, M., Shalamanov-Korobar, L., Sirakov, N., Tzedakis, P.C., 2012. Volcanic ash layers illuminate the resilience of Neanderthals and early modern humans to natural hazards. Proceedings of the National Academy of Sciences 109, 13532-13537.

Lowe, J.J., Bronk Ramsey, C., Housley, R.A., Lane, C.S., Tomlinson, E.L., RESET Team, RESET Associates, 2015. The RESET project: constructing a European tephra lattice for refined synchronisation of environmental and archaeological events during the last c. 100 ka. Quaternary Science Reviews 118, 1-17.

Lowe, J.J., Rasmussen, S.O., Björck, S., Hoek, W.Z., Steffensen, J.P., Walker, M.J.C., Yu, Z.C., the INTIMATE group, 2008. Synchronisation of palaeoenvironmental events in the North Atlantic region during the Last Termination: a revised protocol recommended by the INTIMATE group. Quaternary Science Reviews 27, 6-17.

Lu, H.-Y., Wu, N.-Q., Liu, K.-B., Jiang, H., Liu, T.-S., 2007. Phytoliths as quantitative indicators for the reconstruction of past environmental conditions in China II: palaeoenvironmental reconstruction in the Loess Plateau. Quaternary Science Reviews 26, 759-772.

MacDonald, G.A., Katsura, T. 1964. Chemical composition of Hawaiian lavas. Journal of Petrology 5, 83-133.

Martrat, B., Grimalt, J.O., Shackleton, N.J., de Abreu, L., Hutterli, M.A. and Stocker, T.F., 2007. Four climate cycles of recurring deep and surface water destabilizations on the Iberian Margin. Science 317, 502-507.

Matthews, I.P., Trincardi, F., Lowe, J.J., Bourne, A.J., Macleod, A., Abbott, P.M., Andersen, N., Asioli, A., Blockley, S.P.E., Lane, C.S., Oh, Y.A., Satow, C.S., Staff, R.A., Wulf, S., 2015. Developing a robust tephrochronological framework for Late Quaternary marine records in the Southern Adriatic Sea: new data from core station SA03-11. Quaternary Science Reviews 118, 84-104.

Mortensen, A.K., Bigler, M., Grönvold, K., Steffensen, J.P., Johnsen, S.J., 2005. Volcanic ash layers from the Last Glacial Termination in the NGRIP ice core. Journal of Quaternary Science 20, 209-219.

North Greenland Ice Core Project Members, 2004. High-resolution record of Northern Hemisphere climate extending into the last interglacial period. Nature 431, 147-151.

Rasmussen, T.L., Wastegård, S., Kuijpers, A., van Weering, T.C.E., Heinemeier, J., Thomsen, E., 2003. Stratigraphy and distribution of tephra layers in marine sediment cores from the Faeroe Islands, North Atlantic. Marine Geology 199, 263-277.

Ruddiman W., Glover R., 1972. Vertical mixing of ice-rafted volcanic ash in North Atlantic sediments. Geological Society Bulletin 83, 2817-2836.

Sanchez Goñi, M.F., Harrison, S.P., 2010. Millennial-scale climate variability and vegetation changes during the Last Glacial: concepts and terminology. Quaternary Science Reviews 29, 2823-2827.

Seierstad, I.K., Abbott, P.M., Bigler, M., Blunier, T., Bourne, A.J., Brook, E., Buchardt, S.L., Buizert, C., Clausen, H.B., Cook, E., Dahl-Jensen, D., Davies, S.M., Guillevic, M., Johnsen, S.J., Pedersen, D.S., Popp, T.J., Rasmussen, S.O., Severinghaus, J.P., Svensson, A., Vinther, B.M. (2014). Consistently dated records from the Greenland GRIP, GISP2, and NGRIP ice cores for the past 104 ka reveal millennial-scale $\delta^{18}O$ gradients with possible Heinrich event imprint. Quaternary Science Reviews 106, 29-46.

Timms, R.G.O., Matthews, I.P., Palmer, A.P., Candy, I., Abel, L. (2017) A high-resolution tephrostratigraphy from Quoyloo Meadow, Orkney, Scotland: Implications for the tephrostratigraphy of NW Europe during the Last Glacial-Interglacial Transition. Quaternary Geochronology 40, 67-81.

Tryon, C.A., Logan, M.A.V., Mouralis, D., Kuehn, S., Slimak, L., Balkan-Atl1, N., 2009. Building a tephrostratigraphic framework for the Paleolithic of central Anatolia, Turkey. Journal of Archaeological Science 36, 637-652.

Voelker, A.H.L., Haflidason, H., 2015. Refining the Icelandic tephrachronology of the last glacial period – The deep-sea core PS2644 record from the southern Greenland Sea. Global and Planetary Change 131, 35-62.

Vogelsang, E., Sarnthein, M., Pflaumann, U., 2004. Distribution of planktic foraminifera in sediment core GIK23415-9. DOI:10.1594/PANGAEA.186156.

Wastegård, S., Rasmussen, T.L., 2014. Faroe Marine Ash Zone IV: a new MIS 3 ash zone on the Faroe Islands margin. In Austin, W.E.N., Abbott, P.M., Davies, S.M., Pearce, N.J.G., Wastegård, S., (eds) Marine Tephrochronology, Geological Society of London Special Publication 398, 81-93.

Wastegård S., Rasmussen T.L., Kuijpers A., Nielsen T., van Weering, T.C.E., 2006. Composition and origin of ash zones from Marine Isotope Stages 3 and 2 in the North Atlantic. Quaternary Science Reviews 25, 2409-2419.

Weinelt, M. (2004) Ice rafted debris of sediment core GIK23415-9. DOI:10.1594/PANGAEA.143869.

Zanchetta, G., Sulpizio, R., Roberts, N., Cioni, R., Eastwood, W.J., Siani, G., Caron, B., Paterne, M., Santacroce, R., 2011. Tephrostratigraphy, chronology and climatic events of the Mediterranean basin during the Holocene: An overview. The Holocene 21, 33-52.

Zielinski G.A., Mayewski P.A., Meeker L.D., Gronvöld K., Germani M.S., Whitlow S., Twickler M.S., Taylor K., 1997. Volcanic aerosol records and tephrochronology of the Summit, Greenland, ice cores. Journal of Geophysical Research 102**,** 26,625-26,640.

Zumaque, J., Eynaud, F., Zaragosi, S., Marret, F., Matsuzaki, K.M., Kissel, C., Roche, D.M., Malaize, B., Michel, E., Billy, I., Richter, T., Palis, E., 2012. An ocean-ice coupled response during the last glacial: a view from a marine isotope stage 3 record south of the Faeroe Shetland Gateway. Climate of the Past 8, 1997-2017.

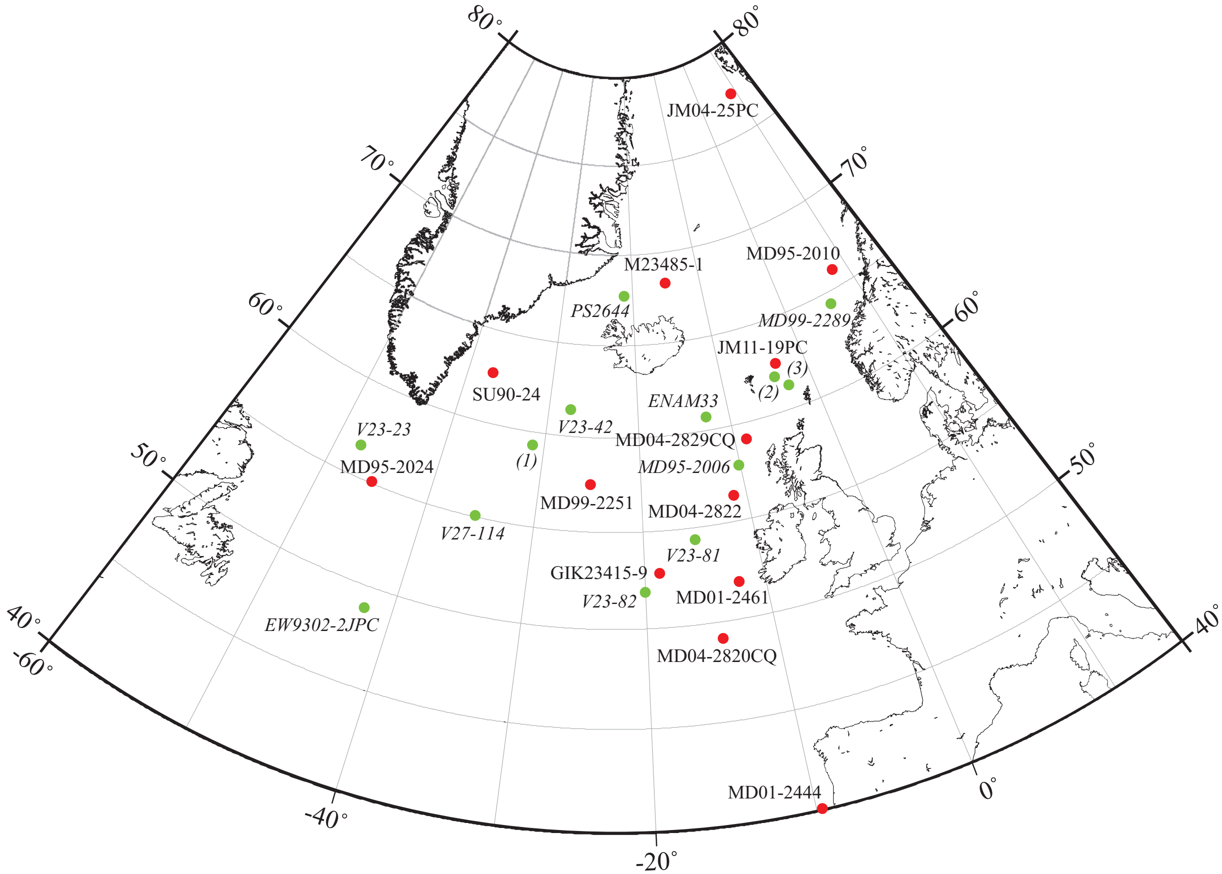

80°
80°
70°
70°
60°
60°
50°
50°
40°
40°
-60°
-40°
-20°
0°
JM04-25PC
M23485-1
MD95-2010
PS2644
MD99-2289
JM11-19PC
(3)
(2)
SU90-24
ENAM33
V23-42
V23-23
MD04-2829CQ
(1)
MD95-2006
MD95-2024
MD99-2251
MD04-2822
V27-114
V23-81
GIK23415-9
MD01-2461
V23-82
EW9302-2JPC
MD04-2820CQ
MD01-2444

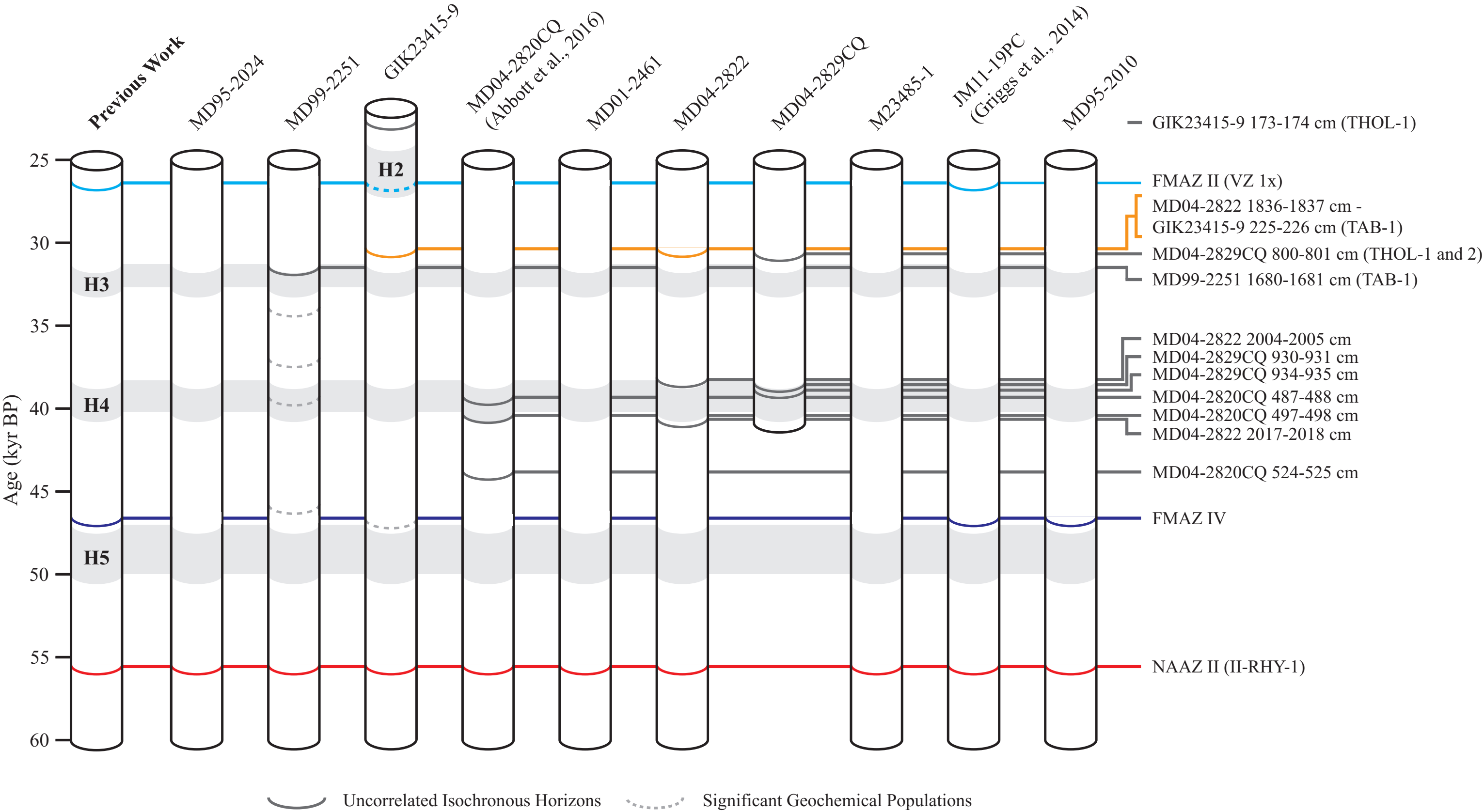

Previous Work
MD95-2024
MD99-2251
GIK23415-9
MD04-2820CQ (Abbott et al., 2016)
MD01-2461
MD04-2822
MD04-2829CQ
M23485-1
JM11-19PC (Griggs et al., 2014)
MD95-2010
H2
H3
H4
H5
Age (kyr BP)
25
30
35
40
45
50
55
60
GIK23415-9 173-174 cm (THOL-1)
FMAZ II (VZ 1x)
MD04-2822 1836-1837 cm -
GIK23415-9 225-226 cm (TAB-1)
MD04-2829CQ 800-801 cm (THOL-1 and 2)
MD99-2251 1680-1681 cm (TAB-1)
MD04-2822 2004-2005 cm
MD04-2829CQ 930-931 cm
MD04-2829CQ 934-935 cm
MD04-2820CQ 487-488 cm
MD04-2820CQ 497-498 cm
MD04-2822 2017-2018 cm
MD04-2820CQ 524-525 cm
FMAZ IV
NAAZ II (II-RHY-1)
Uncorrelated Isochronous Horizons
Significant Geochemical Populations

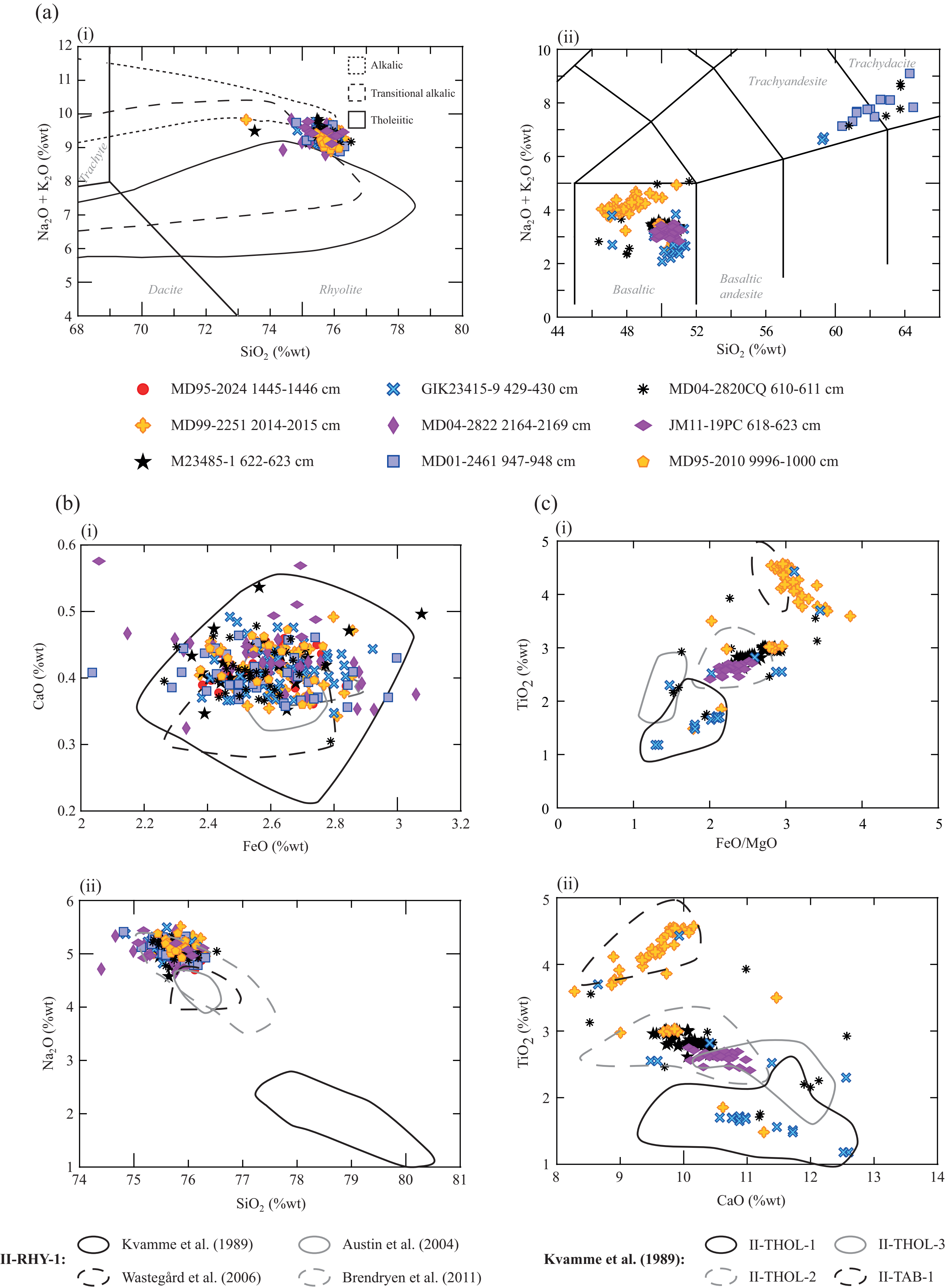

(a)
(i)
Alkalic
Transitional alkalic
Tholeiitic
Trachyte
Dacite
Rhyolite
$Na_2O + K_2O$ (%wt)
SiO_2 (%wt)
(ii)
Trachydacite
Trachyandesite
Basaltic
Basaltic andesite
$Na_2O + K_2O$ (%wt)
SiO_2 (%wt)
MD95-2024 1445-1446 cm
GIK23415-9 429-430 cm
MD04-2820CQ 610-611 cm
MD99-2251 2014-2015 cm
MD04-2822 2164-2169 cm
JM11-19PC 618-623 cm
M23485-1 622-623 cm
MD01-2461 947-948 cm
MD95-2010 9996-1000 cm
(b)
(i)
CaO (%wt)
FeO (%wt)
(c)
(i)
TiO_2 (%wt)
FeO/MgO
(ii)
Na_2O (%wt)
SiO_2 (%wt)
(ii)
TiO_2 (%wt)
CaO (%wt)
II-RHY-1:
Kvamme et al. (1989)
Austin et al. (2004)
Wastegård et al. (2006)
Brendryen et al. (2011)
Kvamme et al. (1989):
II-THOL-1
II-THOL-3
II-THOL-2
II-TAB-1

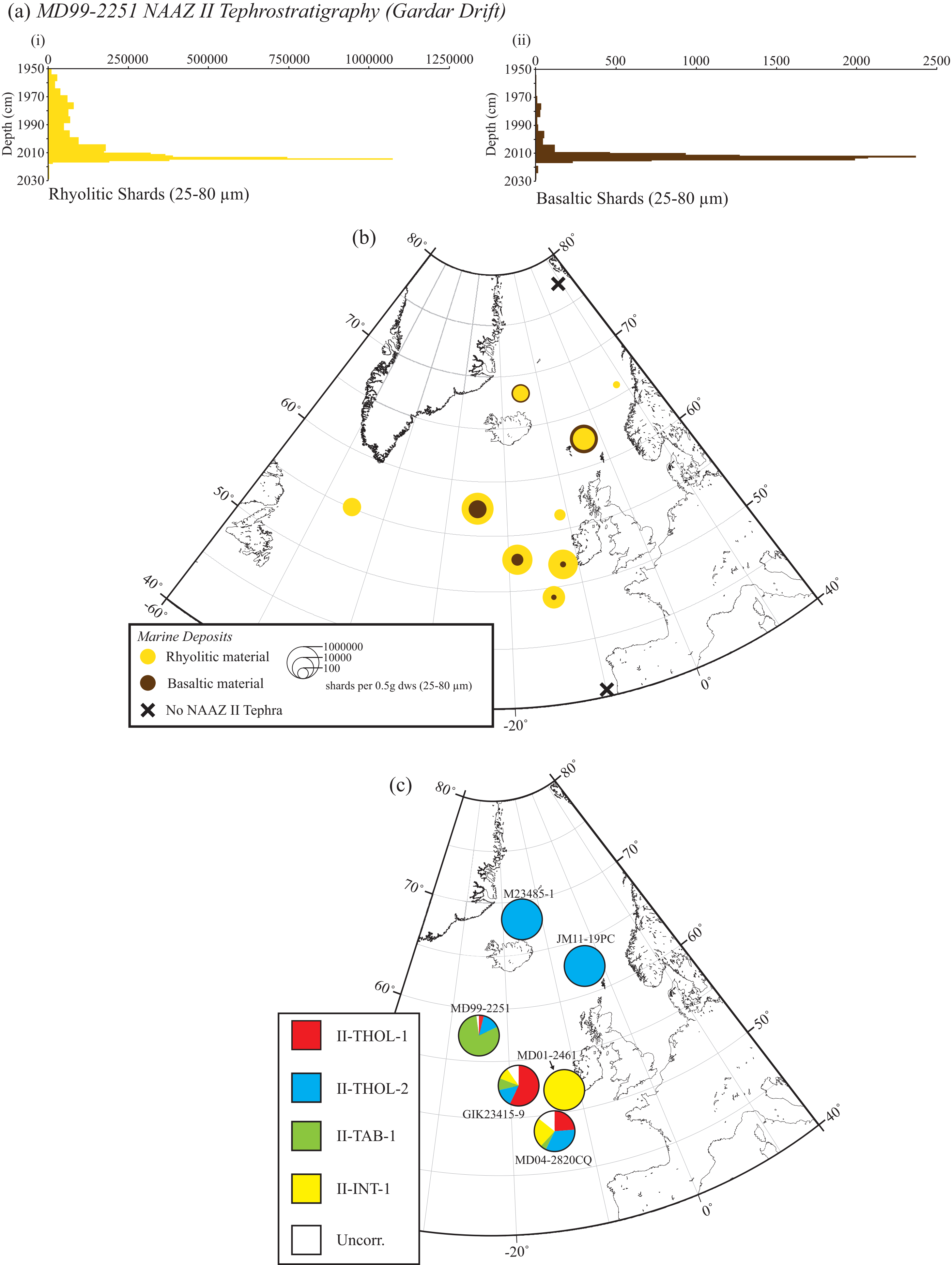

(a) MD99-2251 NAAZ II Tephrostratigraphy (Gardar Drift)
(i)
0
250000
500000
750000
1000000
1250000
1950
1970
1990
2010
2030
Depth (cm)
Rhyolitic Shards (25-80 μm)
(ii)
0
500
1000
1500
2000
2500
1950
1970
1990
2010
2030
Depth (cm)
Basaltic Shards (25-80 μm)
(b)
80°
80°
70°
70°
60°
60°
50°
50°
40°
40°
-60°
0°
-20°
Marine Deposits
Rhyolitic material
Basaltic material
No NAAZ II Tephra
1000000
10000
100
shards per 0.5g dws (25-80 μm)
(c)
80°
80°
70°
70°
60°
60°
50°
40°
0°
-20°
M23485-1
JM11-19PC
MD99-2251
MD01-2461
GIK23415-9
MD04-2820CQ
II-THOL-1
II-THOL-2
II-TAB-1
II-INT-1
Uncorr.

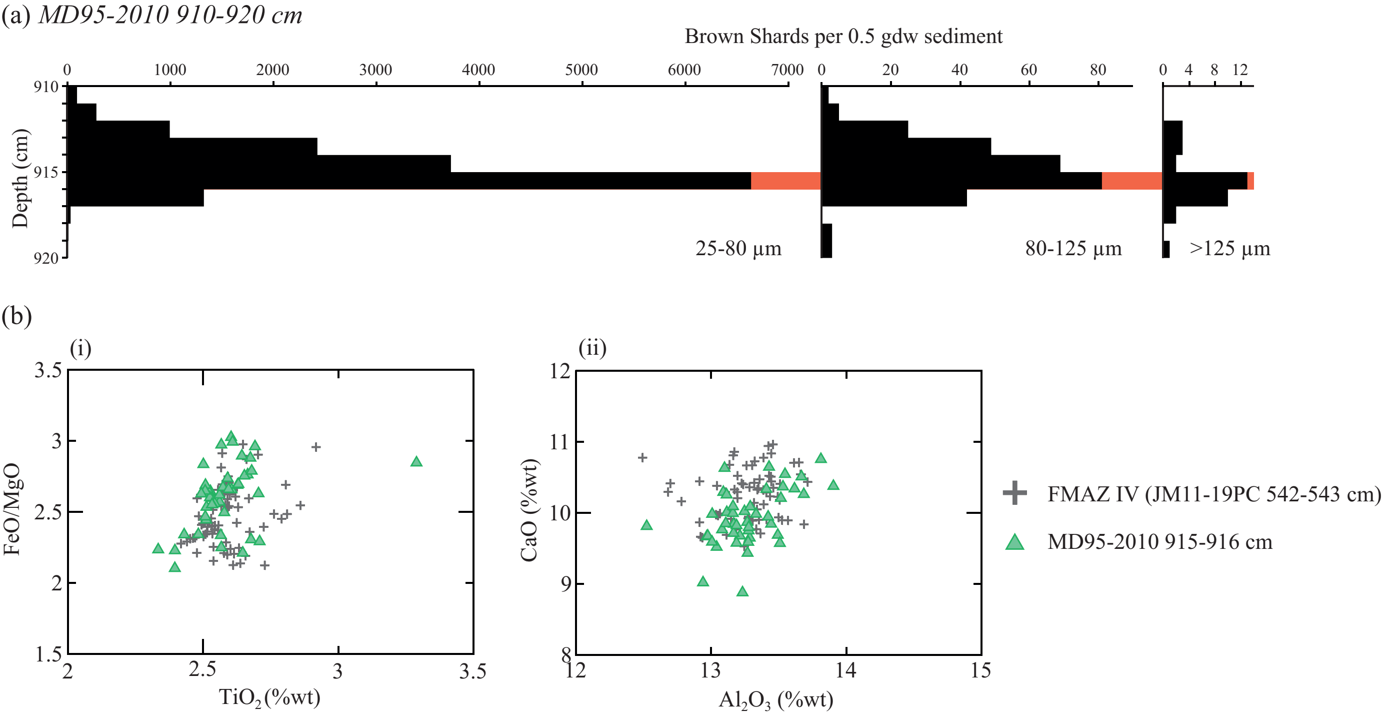

(a) MD95-2010 910-920 cm
Brown Shards per 0.5 gdw sediment
0
1000
2000
3000
4000
5000
6000
7000
0
20
40
60
80
0
4
8
12
910
915
920
Depth (cm)
25-80 µm
80-125 µm
>125 µm
(b)
(i)
3.5
3
2.5
2
1.5
2
2.5
3
3.5
FeO/MgO
TiO2 (%wt)
(ii)
12
11
10
9
8
12
13
14
15
CaO (%wt)
Al2O3 (%wt)
FMAZ IV (JM11-19PC 542-543 cm)
MD95-2010 915-916 cm

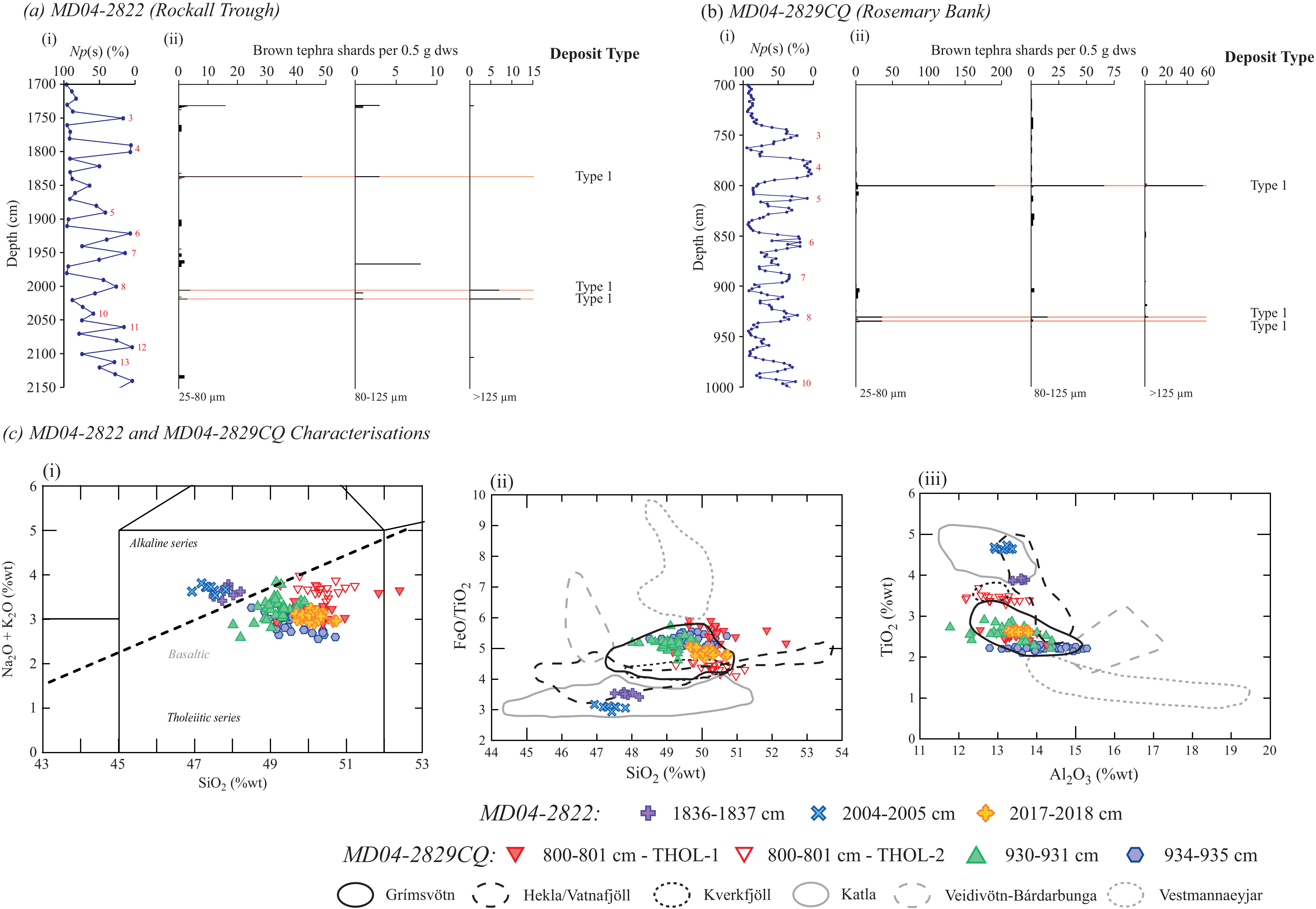
(a) MD04-2822 (Rockall Trough)
(i)
Np(s) (%)
Depth (cm)
(ii)
Brown tephra shards per 0.5 g dws
Deposit Type
Type 1
Type 1
Type 1
25-80 µm
80-125 µm
>125 µm
(b) MD04-2829CQ (Rosemary Bank)
(i)
Np(s) (%)
Depth (cm)
(ii)
Brown tephra shards per 0.5 g dws
Deposit Type
Type 1
Type 1
Type 1
25-80 µm
80-125 µm
>125 µm
(c) MD04-2822 and MD04-2829CQ Characterisations
(i)
Alkaline series
Basaltic
Tholeiitic series
$Na_2O + K_2O$ (%wt)
SiO_2 (%wt)
(ii)
FeO/TiO_2
SiO_2 (%wt)
(iii)
TiO_2 (%wt)
Al_2O_3 (%wt)
MD04-2822:
1836-1837 cm
2004-2005 cm
2017-2018 cm
MD04-2829CQ:
800-801 cm - THOL-1
800-801 cm - THOL-2
930-931 cm
934-935 cm
Grímsvötn
Hekla/Vatnafjöll
Kverkfjöll
Katla
Veidivötn-Bárdarbunga
Vestmannaeyjar

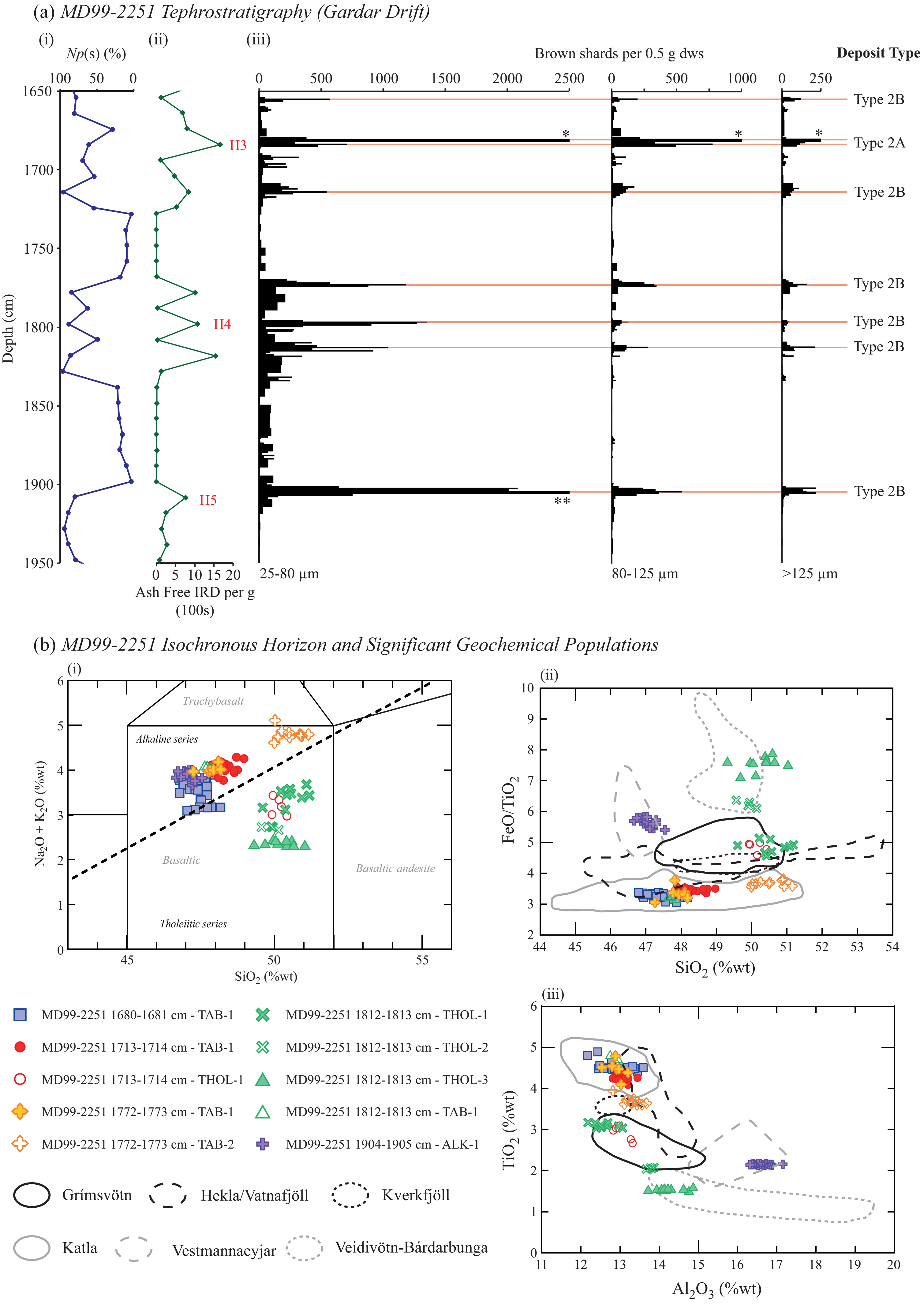

(a) MD99-2251 Tephrostratigraphy (Gardar Drift)
(i)
Np(s) (%)
(ii)
(iii)
Brown shards per 0.5 g dws
Deposit Type
Depth (cm)
H3
H4
H5
Ash Free IRD per g (100s)
25-80 µm
80-125 µm
>125 µm
Type 2B
Type 2A
Type 2B
Type 2B
Type 2B
Type 2B
Type 2B
(b) MD99-2251 Isochronous Horizon and Significant Geochemical Populations
(i)
Trachybasalt
Alkaline series
Basaltic
Basaltic andesite
Tholeiitic series
Na2O + K2O (%wt)
SiO2 (%wt)
(ii)
FeO/TiO2
SiO2 (%wt)
(iii)
TiO2 (%wt)
Al2O3 (%wt)
MD99-2251 1680-1681 cm - TAB-1
MD99-2251 1713-1714 cm - TAB-1
MD99-2251 1713-1714 cm - THOL-1
MD99-2251 1772-1773 cm - TAB-1
MD99-2251 1772-1773 cm - TAB-2
MD99-2251 1812-1813 cm - THOL-1
MD99-2251 1812-1813 cm - THOL-2
MD99-2251 1812-1813 cm - THOL-3
MD99-2251 1812-1813 cm - TAB-1
MD99-2251 1904-1905 cm - ALK-1
Grímsvötn
Hekla/Vatnafjöll
Kverkfjöll
Katla
Vestmannaeyjar
Veidivötn-Bárdarbunga

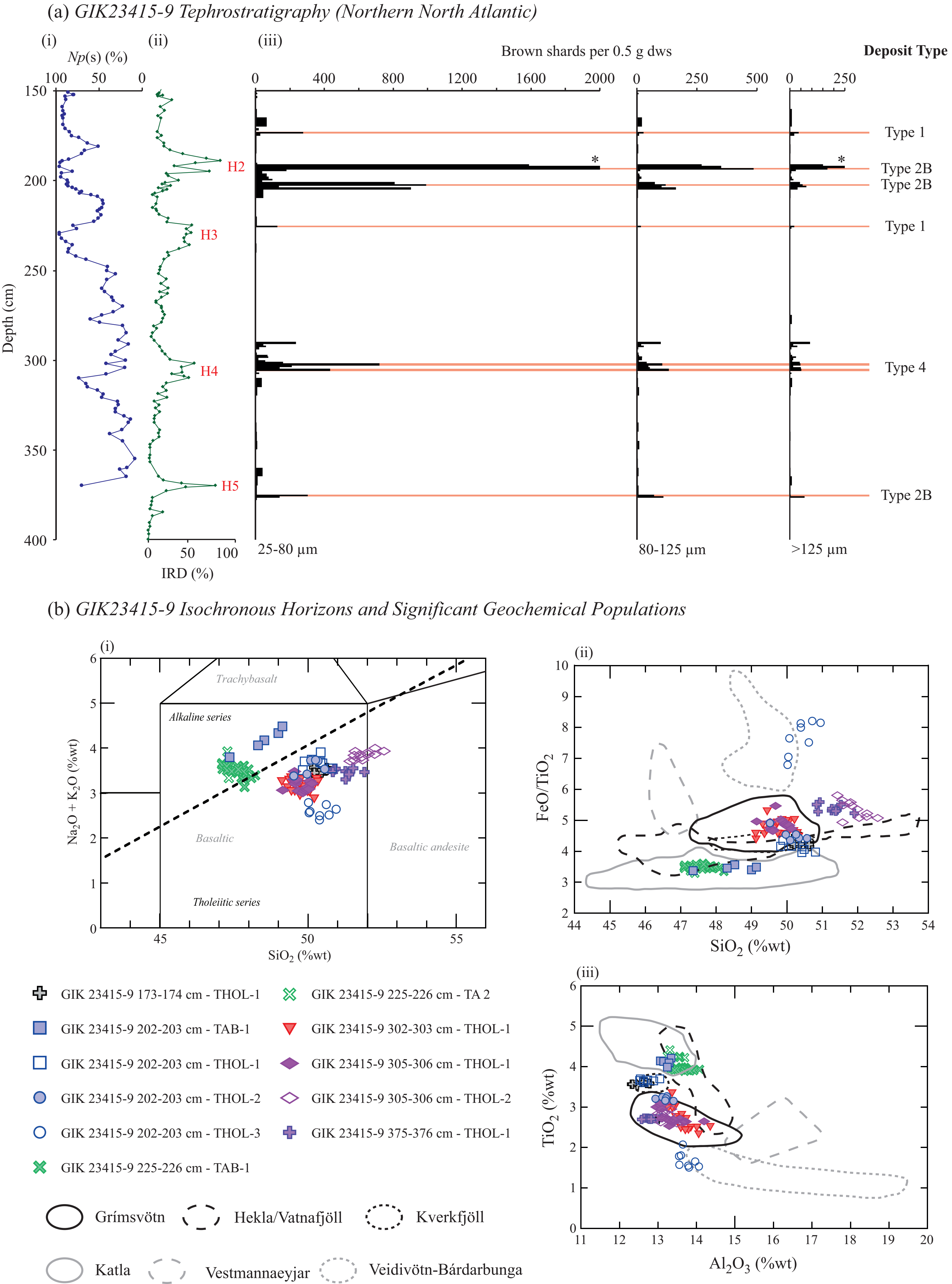

(a) GIK23415-9 Tephrostratigraphy (Northern North Atlantic)
(i)
(ii)
(iii)
Np(s) (%)
100 50 0
Depth (cm)
150 200 250 300 350 400
0 50 100
IRD (%)
H2
H3
H4
H5
Brown shards per 0.5 g dws
0 400 800 1200 1600 2000
0 250 500
0 250
*
25-80 µm
80-125 µm
>125 µm
Deposit Type
Type 1
Type 2B
Type 2B
Type 1
Type 4
Type 2B
(b) GIK23415-9 Isochronous Horizons and Significant Geochemical Populations
(i)
Trachybasalt
Alkaline series
Basaltic
Tholeiitic series
Basaltic andesite
$Na_2O + K_2O$ (%wt)
SiO_2 (%wt)
45 50 55
(ii)
FeO/TiO_2
SiO_2 (%wt)
44 45 46 47 48 49 50 51 52 53 54
(iii)
TiO_2 (%wt)
Al_2O_3 (%wt)
11 12 13 14 15 16 17 18 19 20
GIK 23415-9 173-174 cm - THOL-1
GIK 23415-9 202-203 cm - TAB-1
GIK 23415-9 202-203 cm - THOL-1
GIK 23415-9 202-203 cm - THOL-2
GIK 23415-9 202-203 cm - THOL-3
GIK 23415-9 225-226 cm - TAB-1
GIK 23415-9 225-226 cm - TA 2
GIK 23415-9 302-303 cm - THOL-1
GIK 23415-9 305-306 cm - THOL-1
GIK 23415-9 305-306 cm - THOL-2
GIK 23415-9 375-376 cm - THOL-1
Grímsvötn
Hekla/Vatnafjöll
Kverkfjöll
Katla
Vestmannaeyjar
Veidivötn-Bárdarbunga

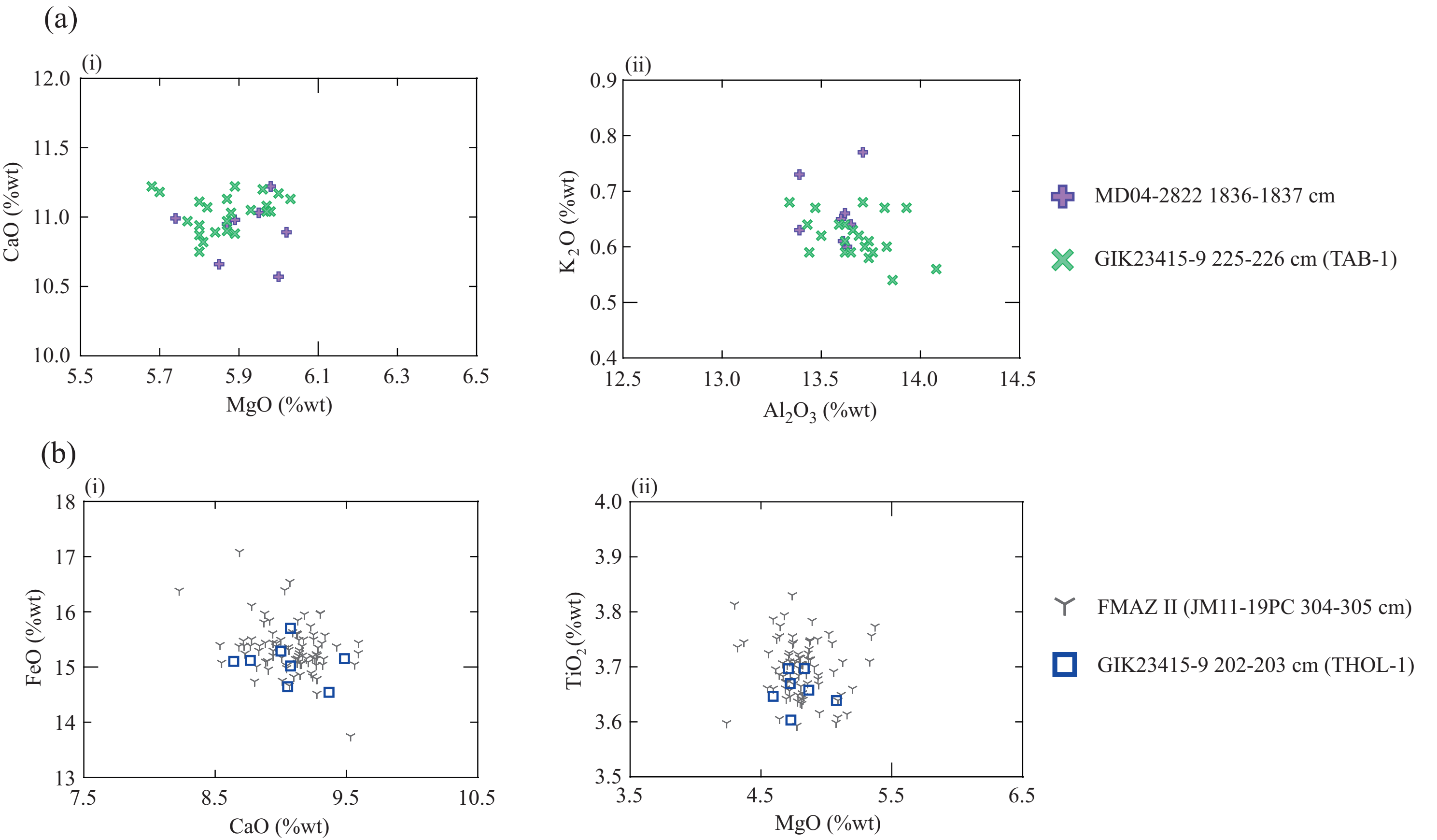

(a)
(i)
CaO (%wt)
MgO (%wt)
12.0
11.5
11.0
10.5
10.0
5.5
5.7
5.9
6.1
6.3
6.5
(ii)
K_2O (%wt)
Al_2O_3 (%wt)
0.9
0.8
0.7
0.6
0.5
0.4
12.5
13.0
13.5
14.0
14.5
MD04-2822 1836-1837 cm
GIK23415-9 225-226 cm (TAB-1)
(b)
(i)
FeO (%wt)
CaO (%wt)
18
17
16
15
14
13
7.5
8.5
9.5
10.5
(ii)
TiO_2 (%wt)
MgO (%wt)
4.0
3.9
3.8
3.7
3.6
3.5
3.5
4.5
5.5
6.5
FMAZ II (JM11-19PC 304-305 cm)
GIK23415-9 202-203 cm (THOL-1)

Tephra Horizon/Deposit (Pop.)	Climatic Event	Composition	Volcanic Source	Deposit Type	Ref(s)
Isochronous Horizons					
GIK23415-9 173-174 cm (THOL-1)	Post H2	Tholeiitic bas	Kverkfjöll	1	1
FMAZ II	Post DO-3	Transitional alkali bas	Hekla/Vatnafjöll	2A	2, 3, 4, 5
MD04-2822 1836-1837 cm	Pre DO-4	Transitional alkali bas	Katla or Hekla/Vatnafjöll	1	1
GIK23415-9 225-226 cm (TAB-1)	H3	Transitional alkali bas	Katla or Hekla/Vat.	1	1
MD04-2829CQ 800-801 cm (THOL-1)	Pre DO-4	Tholeiitic bas	Grímsvötn	1	1
MD04-2829CQ 800-801 cm (THOL-2)	Pre DO-4	Tholeiitic bas	Kverkfjöll	1	1
MD99-2251 1680-1681 cm (TAB-1)	H3	Transitional alkali bas	Katla	2A	1
MD04-2822 2004-2005 cm	DO-8	Transitional alkali bas	Katla	1	1
MD04-2829CQ 930-931 cm	DO-8	Tholeiitic bas	Grímsvötn	1	1
MD04-2829CQ 934-935 cm	Pre DO-8	Tholeiitic bas	Grímsvötn	1	1
MD04-2820CQ 487-488 cm	Pre DO-8 (H4)	Tholeiitic bas	Grímsvötn	2A	6
MD04-2820CQ 497-498 cm	Pre DO-9	Transitional alkali rhy	Katla	2A	6
MD04-2822 2017-2018 cm	Pre DO-9	Tholeiitic bas	Grímsvötn	1	1
MD04-2820CQ 524-525 cm	Pre DO-11	Tholeiitic bas	Grímsvötn or Kverkfjöll	2A	6
FMAZ IV	Pre DO-12	Tholeiitic bas	Grímsvötn	2A	5, 7
NAAZ II (II-RHY-1)	End of DO-15	Transitional alkali rhy	Tindfjallajökull	3	1, 3, 8, 9, 10
Significant Geochemical Populations					
GIK23415-9 202-203 cm (TAB-1)	*Pre H2*	*Transitional alkali bas*	*Katla*	*2B*	*1*
GIK23415-9 202-203 cm (THOL-1)	*Pre H2*	*Tholeiitic bas*	*Kverkfjöll*	*2B*	*1*
GIK23415-9 202-203 cm (THOL-2)	*Pre H2*	*Tholeiitic bas*	*Grímsvötn*	*2B*	*1*
GIK23415-9 202-203 cm (THOL-3)	*Pre H2*	*Tholeiitic bas*	*Veid. -Bárd.*	*2B*	*1*
MD99-2251 1713-1714 cm (TAB-1)	*Pre H3*	*Transitional alkali bas*	*Katla*	*2B*	*1*
MD99-2251 1713-1714 cm (THOL-1)	*Pre H3*	*Tholeiitic bas*	*Grímsvötn*	*2B*	*1*
MD99-2251 1772-1773 cm (TAB-1)	*Post H4*	*Transitional alkali bas*	*Katla*	*2B*	*1*
MD99-2251 1772-1773 cm (TAB-2)	*Post H4*	*Transitional alkali bas*	*Katla (?)*	*2B*	*1*
GIK23415-9 302-306 cm (THOL-1)	*H4*	*Tholeiitic bas*	*Grímsvötn*	*4*	*1*
GIK23415-9 302-306 cm (THOL-2)	*H4*	*Tholeiitic bas*	*Grímsvötn (?)*	*4*	*1*
MD99-2251 1812-1813 cm (THOL-1)	*H4*	*Tholeiitic bas*	*Grímsvötn*	*2B*	*1*
MD99-2251 1812-1813 cm (THOL-2)	*H4*	*Tholeiitic bas*	*Veid. -Bárd.*	*2B*	*1*
MD99-2251 1812-1813 cm (THOL-3)	*H4*	*Tholeiitic bas*	*Veid. -Bárd.*	*2B*	*1*
MD99-2251 1812-1813 cm (TAB-1)	*H4*	*Transitional alkali bas*	*Katla*	*2B*	*1*
MD99-2251 1904-1905 cm (ALK-1)	*Post H5*	*Alkali bas*	*Vestmannaeyjar*	*2B*	*1*
GIK23415-9 375-376 cm (THOL-1)	*Pre H5*	*Tholeiitic bas*	*Grímsvötn*	*2B*	*1*

Table 1: Summary of isochronous horizons and significant geochemical populations forming the marine tephra framework for the North Atlantic between 25-60 ka BP. The designation of climatic events is based on pre-existing stratigraphic frameworks for the cores. The stratigraphic ordering of horizons between cores is approximate. FMAZ II, FMAZ IV and NAAZ II have been identified in multiple cores. H = Heinrich Event; DO = Dansgaard-Oeschger Event. bas = basaltic; rhy = rhyolitic. Vat. = Vatnafjöll; Veid.-Bárd. = Veidivötn-Bárdarbunga. Deposit types based on the classification scheme outlined in Abbott et al. (submitted). References are as follows: 1: this study; 2: Rasmussen et al. (2003); 3: Wastegård et al. (2006); 4: Davies et al. (2008); 5: Griggs et al. (2014); 6: Abbott et al. (2016); 7: Wastegård and Rasmussen (2014); 8: Kvamme et al. (1989); 9: Austin et al. (2004); 10: Brendryen et al. (2010).

Supplementary Figures

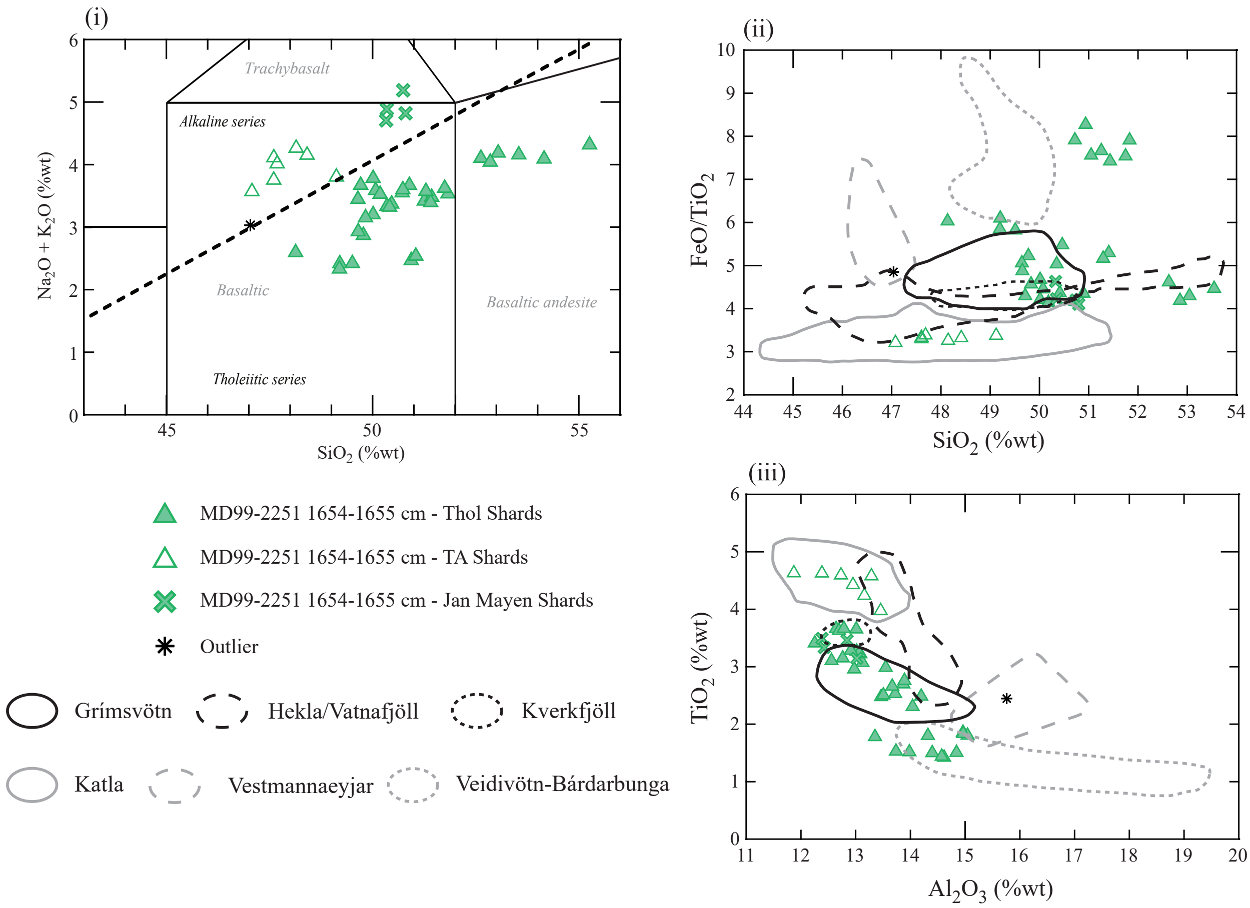

Figure S1: Geochemical populations identified within shard analyses from the MD99-2251 1654-1655 cm deposit. (i) inset of total alkali vs. silica plot. Division line to separate alkaline and sub-alkaline material from MacDonald and Katsura (1964). Chemical classification and nomenclature after Le Maitre et al. (1989). (ii) FeO/TiO_2 vs. SiO_2 and (iii) TiO_2 vs. Al_2O_3 compositional variation diagrams comparing populations to characterisations of proximal Icelandic material. Geochemical fields for Icelandic source volcanoes are based on those utilised in Bourne et al. (2015) and references within.

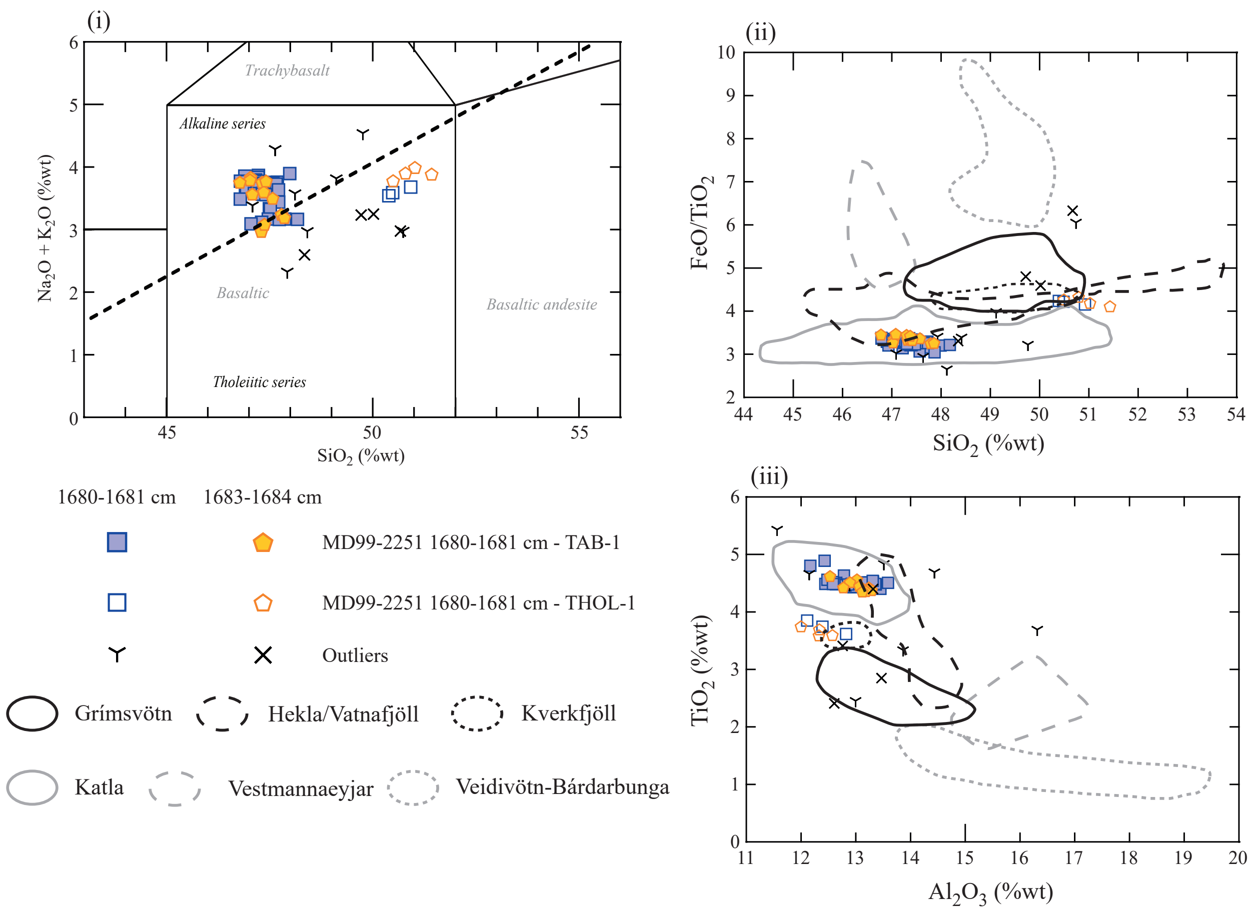

Figure S2: Geochemical populations identified within shard analyses from the MD99-2251 1680-1681 cm deposit. (i) inset of total alkali vs. silica plot. Division line to separate alkaline and sub-alkaline material from MacDonald and Katsura (1964). Chemical classification and nomenclature after Le Maitre et al. (1989). (ii) FeO/TiO_2 vs. SiO_2 and (iii) TiO_2 vs. Al_2O_3 compositional variation diagrams comparing populations to characterisations of proximal Icelandic material. Geochemical fields for Icelandic source volcanoes are based on those utilised in Bourne et al. (2015) and references within.

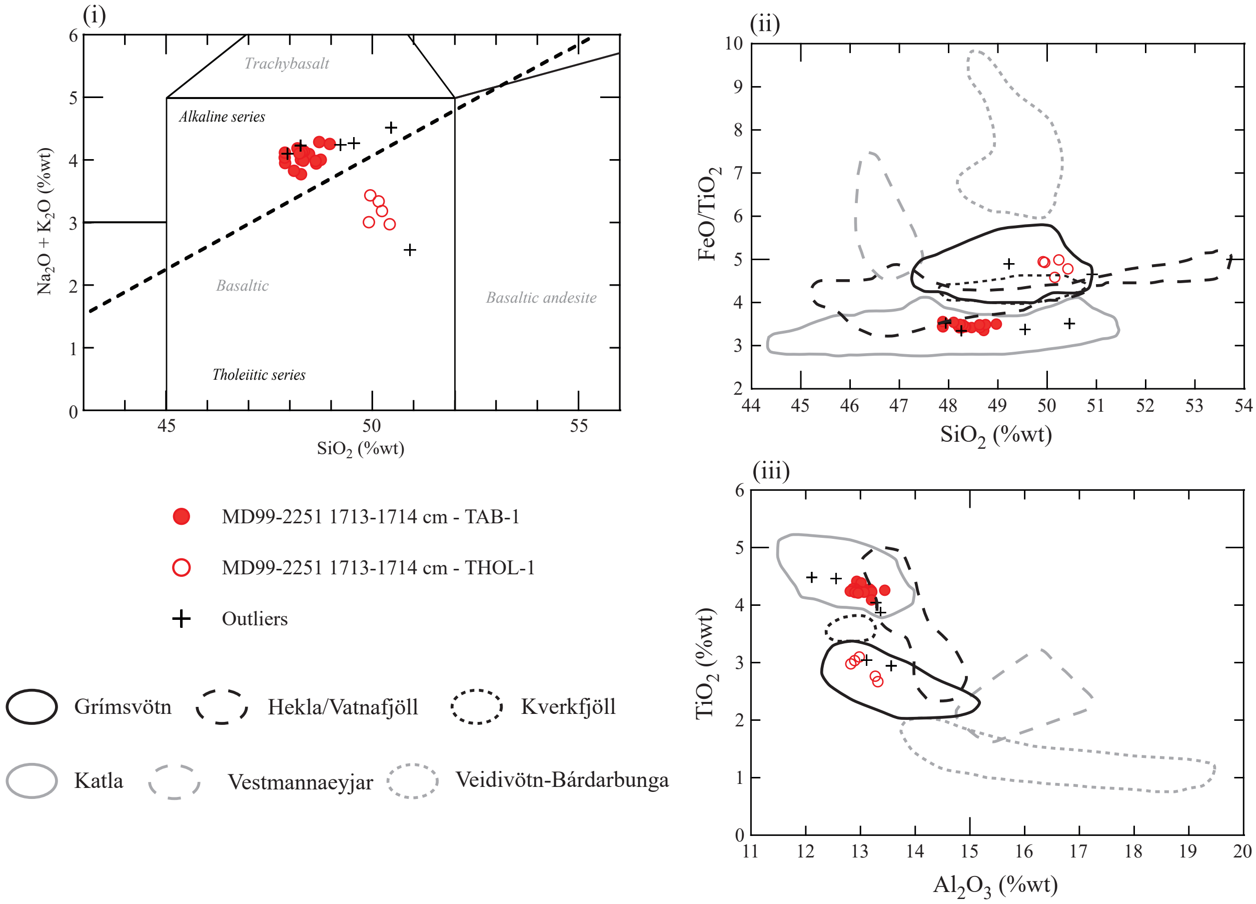

Figure S3: Geochemical populations identified within shard analyses from the MD99-2251 1713-1714 cm deposit. (i) inset of total alkali vs. silica plot. Division line to separate alkaline and sub-alkaline material from MacDonald and Katsura (1964). Chemical classification and nomenclature after Le Maitre et al. (1989). (ii) FeO/TiO_2 vs. SiO_2 and (iii) TiO_2 vs. Al_2O_3 compositional variation diagrams comparing populations to characterisations of proximal Icelandic material. Geochemical fields for Icelandic source volcanoes are based on those utilised in Bourne et al. (2015) and references within.

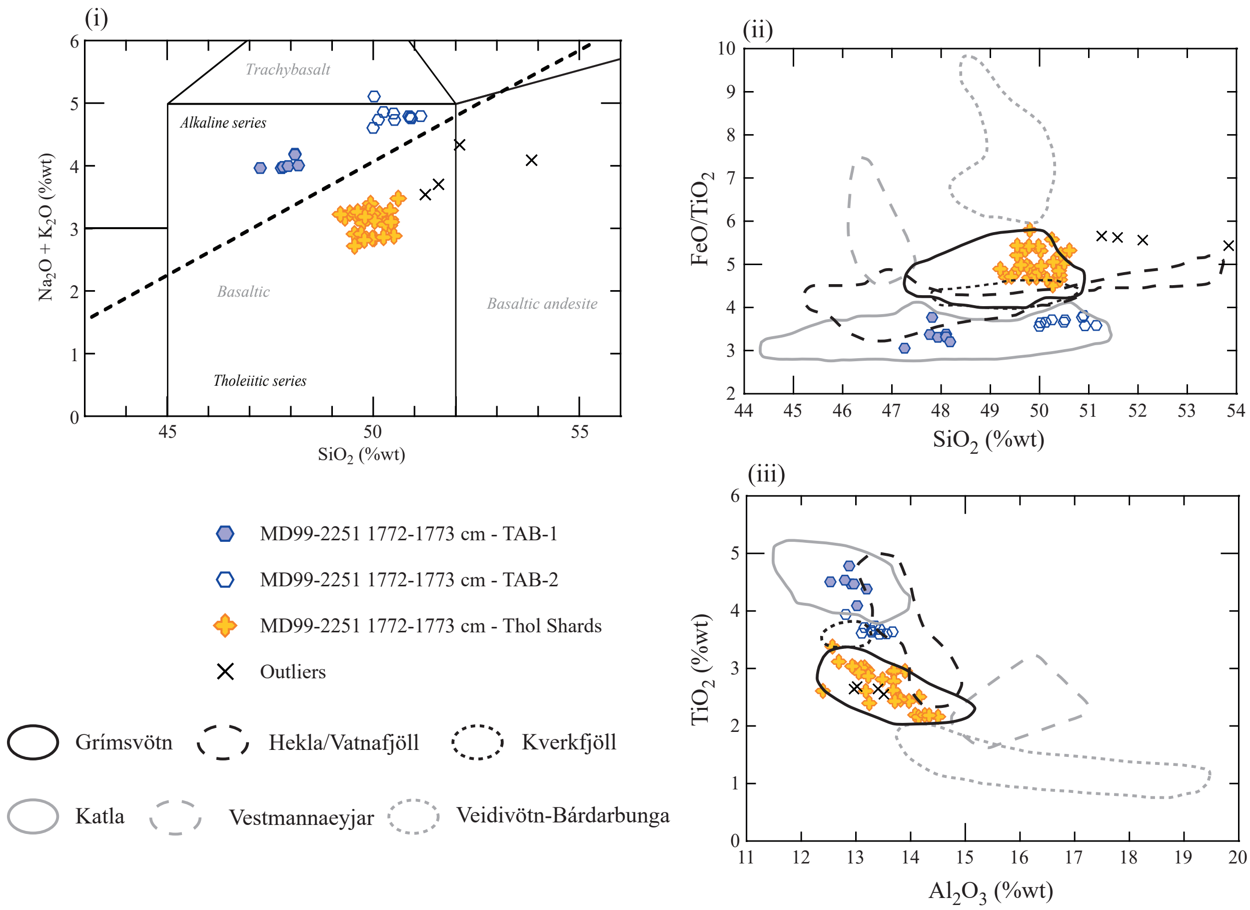

Figure S4: Geochemical populations identified within shard analyses from the MD99-2251 1772-1773 cm deposit. (i) inset of total alkali vs. silica plot. Division line to separate alkaline and sub-alkaline material from MacDonald and Katsura (1964). Chemical classification and nomenclature after Le Maitre et al. (1989). (ii) FeO/TiO_2 vs. SiO_2 and (iii) TiO_2 vs. Al_2O_3 compositional variation diagrams comparing populations to characterisations of proximal Icelandic material. Geochemical fields for Icelandic source volcanoes are based on those utilised in Bourne et al. (2015) and references within.

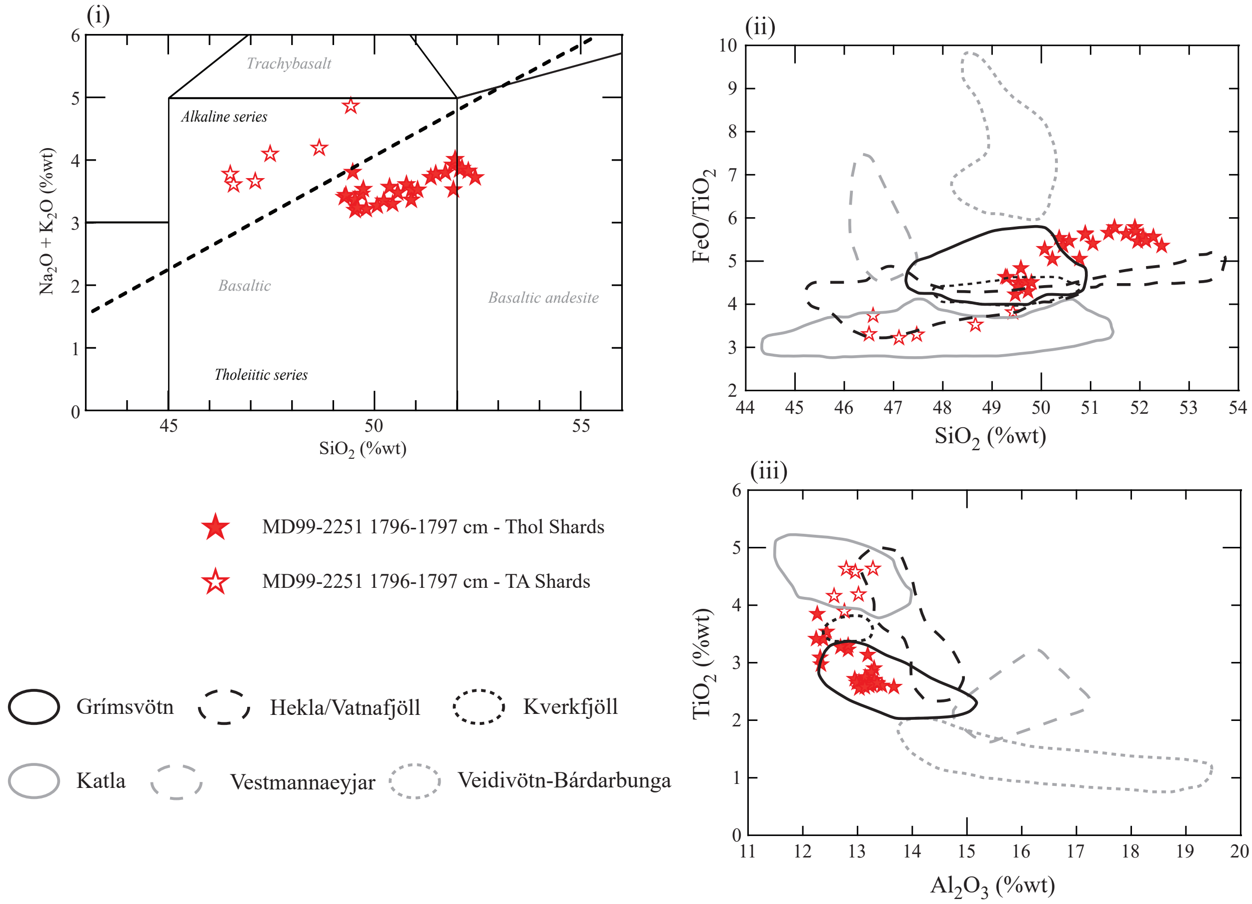

Figure S5: Geochemical populations identified within shard analyses from the MD99-2251 1796-1797 cm deposit. (i) inset of total alkali vs. silica plot. Division line to separate alkaline and sub-alkaline material from MacDonald and Katsura (1964). Chemical classification and nomenclature after Le Maitre et al. (1989). (ii) FeO/TiO_2 vs. SiO_2 and (iii) TiO_2 vs. Al_2O_3 compositional variation diagrams comparing populations to characterisations of proximal Icelandic material. Geochemical fields for Icelandic source volcanoes are based on those utilised in Bourne et al. (2015) and references within.

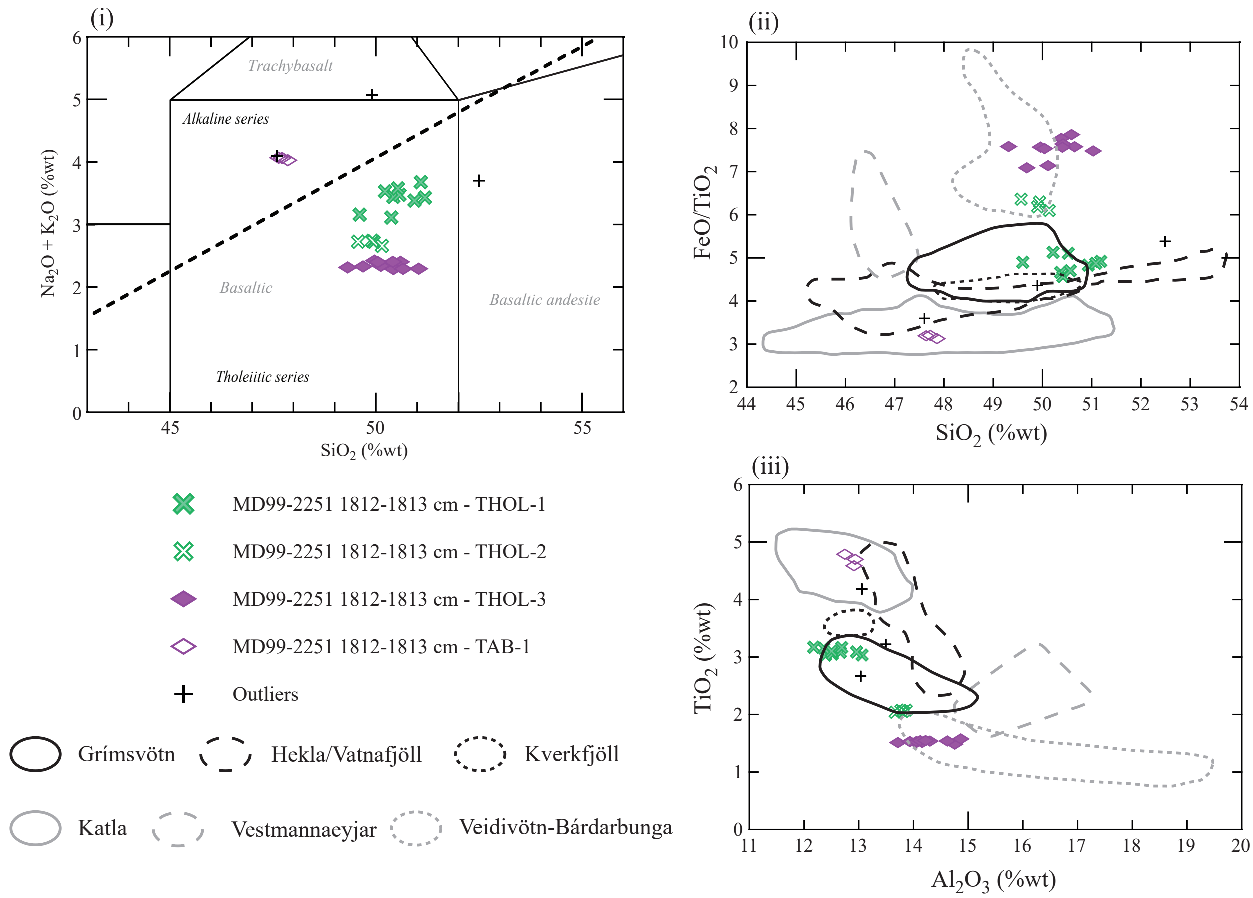

Figure S6: Geochemical populations identified within shard analyses from the MD99-2251 1812-1813 cm deposit. (i) inset of total alkali vs. silica plot. Division line to separate alkaline and sub-alkaline material from MacDonald and Katsura (1964). Chemical classification and nomenclature after Le Maitre et al. (1989). (ii) FeO/TiO_2 vs. SiO_2 and (iii) TiO_2 vs. Al_2O_3 compositional variation diagrams comparing populations to characterisations of proximal Icelandic material. Geochemical fields for Icelandic source volcanoes are based on those utilised in Bourne et al. (2015) and references within.

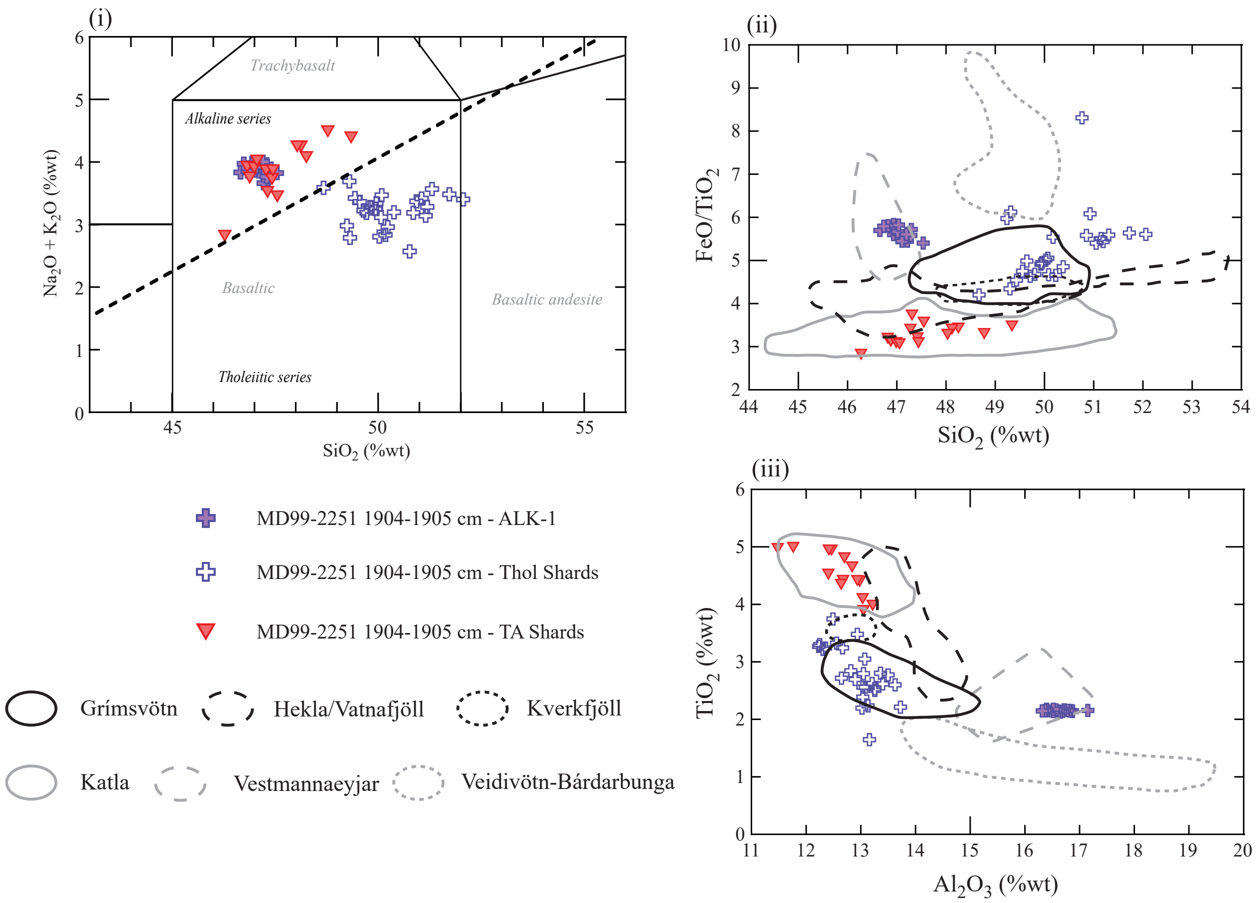

Figure S7: Geochemical populations identified within shard analyses from the MD99-2251 1904-1905 cm deposit. (i) inset of total alkali vs. silica plot. Division line to separate alkaline and sub-alkaline material from MacDonald and Katsura (1964). Chemical classification and nomenclature after Le Maitre et al. (1989). (ii) FeO/TiO_2 vs. SiO_2 and (iii) TiO_2 vs. Al_2O_3 compositional variation diagrams comparing populations to characterisations of proximal Icelandic material. Geochemical fields for Icelandic source volcanoes are based on those utilised in Bourne et al. (2015) and references within.

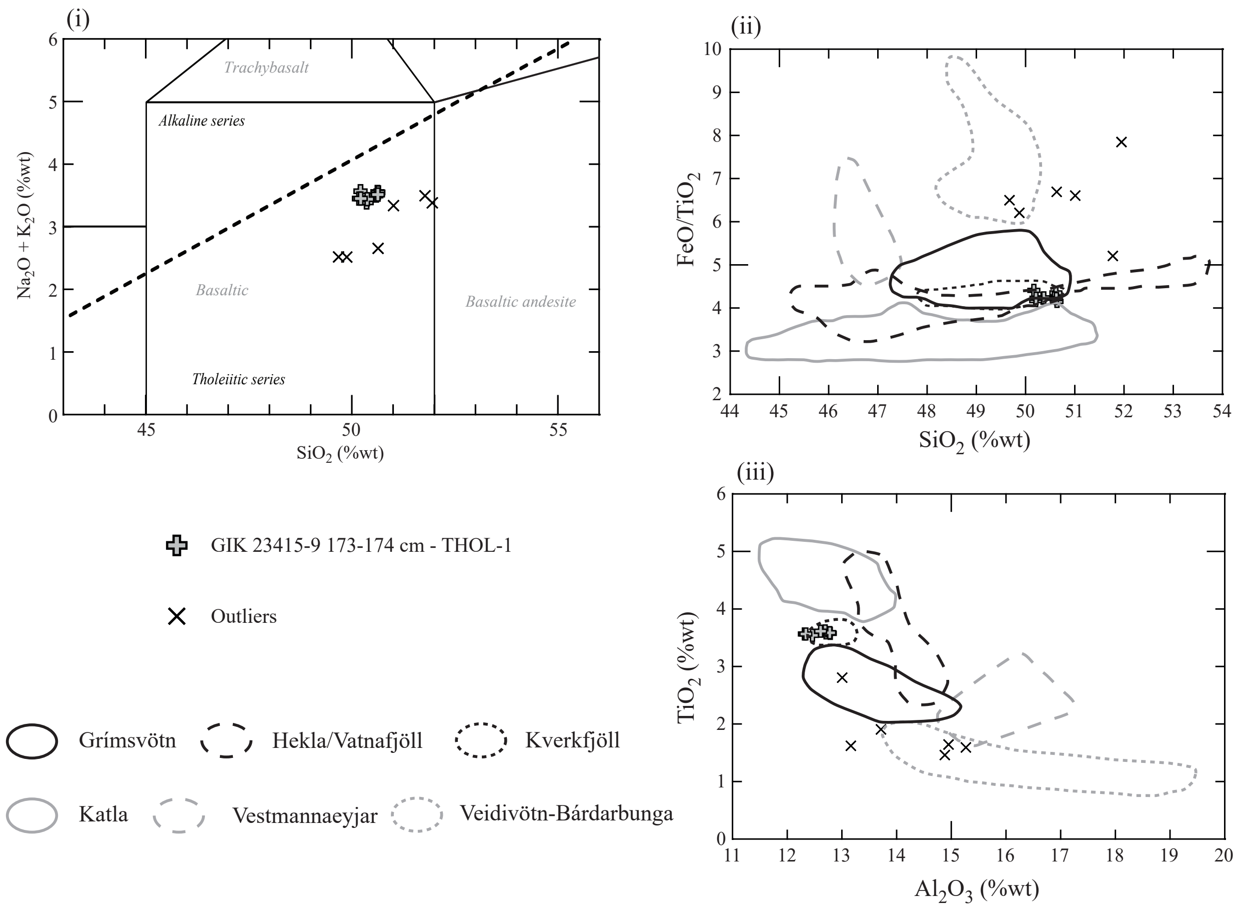

Figure S8: Geochemical populations identified within shard analyses from the GIK23415-9 173-174 cm deposit. (i) inset of total alkali vs. silica plot. Division line to separate alkaline and sub-alkaline material from MacDonald and Katsura (1964). Chemical classification and nomenclature after Le Maitre et al. (1989). (ii) FeO/TiO_2 vs. SiO_2 and (iii) TiO_2 vs. Al_2O_3 compositional variation diagrams comparing populations to characterisations of proximal Icelandic material. Geochemical fields for Icelandic source volcanoes are based on those utilised in Bourne et al. (2015) and references within.

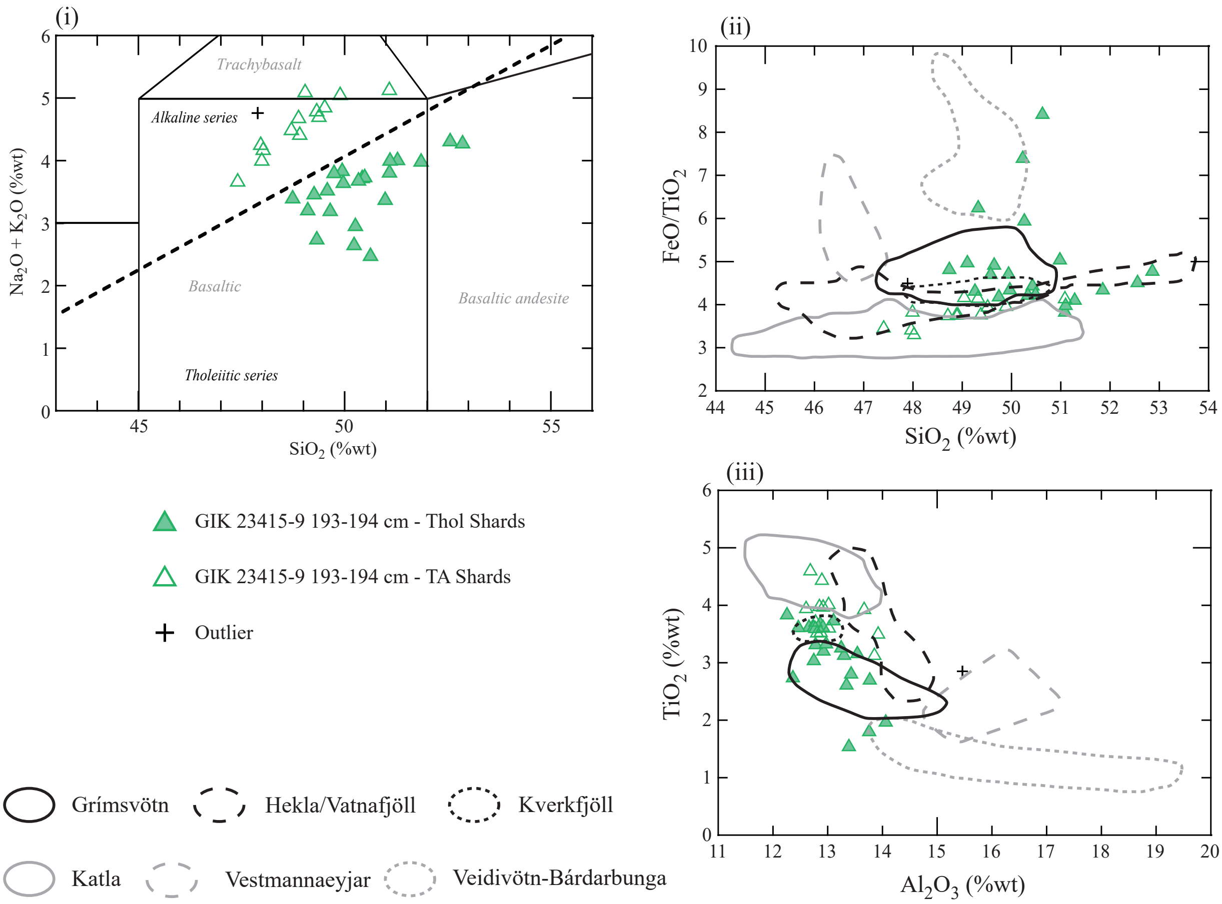

Figure S9: Geochemical populations identified within shard analyses from the GIK23415-9 193-194 cm deposit. (i) inset of total alkali vs. silica plot. Division line to separate alkaline and sub-alkaline material from MacDonald and Katsura (1964). Chemical classification and nomenclature after Le Maitre et al. (1989). (ii) FeO/TiO_2 vs. SiO_2 and (iii) TiO_2 vs. Al_2O_3 compositional variation diagrams comparing populations to characterisations of proximal Icelandic material. Geochemical fields for Icelandic source volcanoes are based on those utilised in Bourne et al. (2015) and references within.

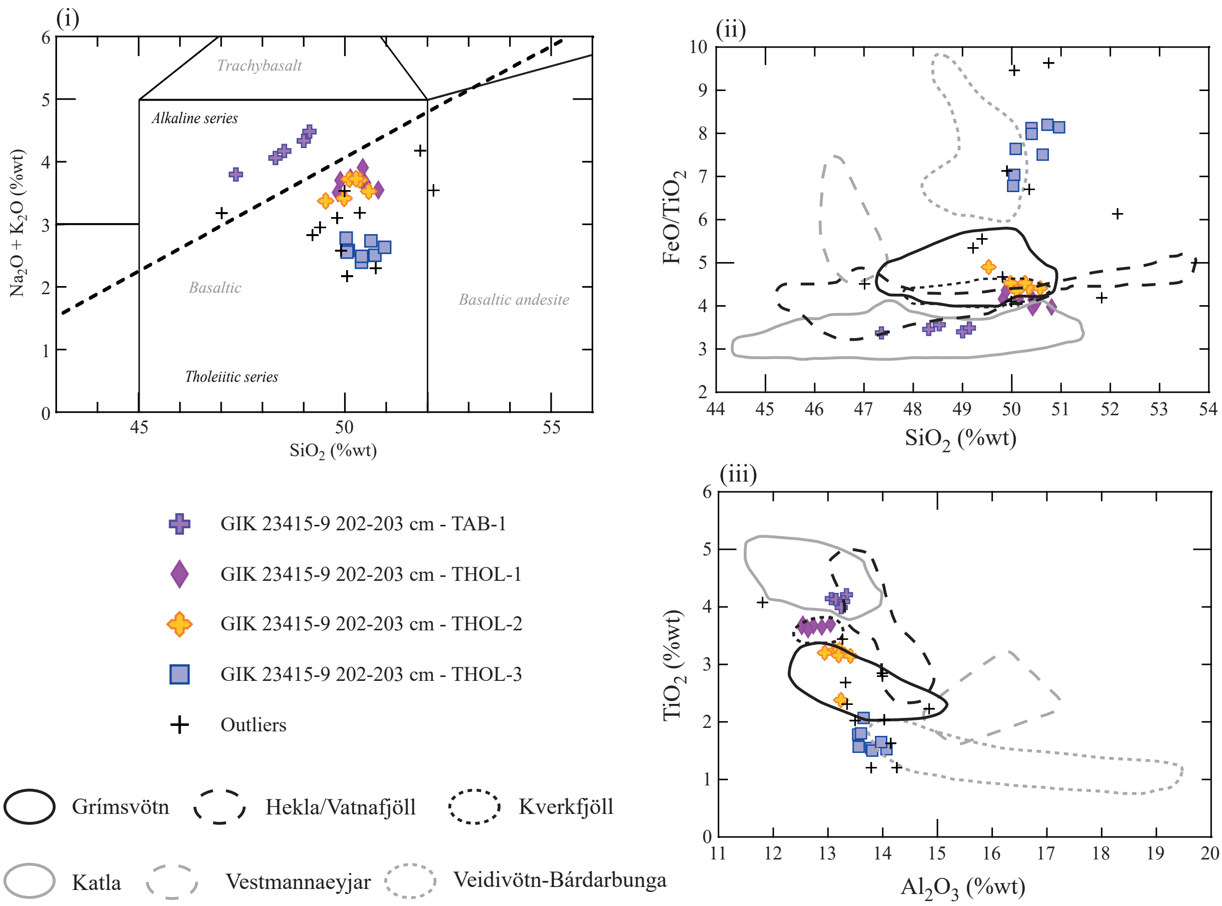

Figure S10: Geochemical populations identified within shard analyses from the GIK23415-9 202-203 cm deposit. (i) inset of total alkali vs. silica plot. Division line to separate alkaline and sub-alkaline material from MacDonald and Katsura (1964). Chemical classification and nomenclature after Le Maitre et al. (1989). (ii) FeO/TiO_2 vs. SiO_2 and (iii) TiO_2 vs. Al_2O_3 compositional variation diagrams comparing populations to characterisations of proximal Icelandic material. Geochemical fields for Icelandic source volcanoes are based on those utilised in Bourne et al. (2015) and references within.

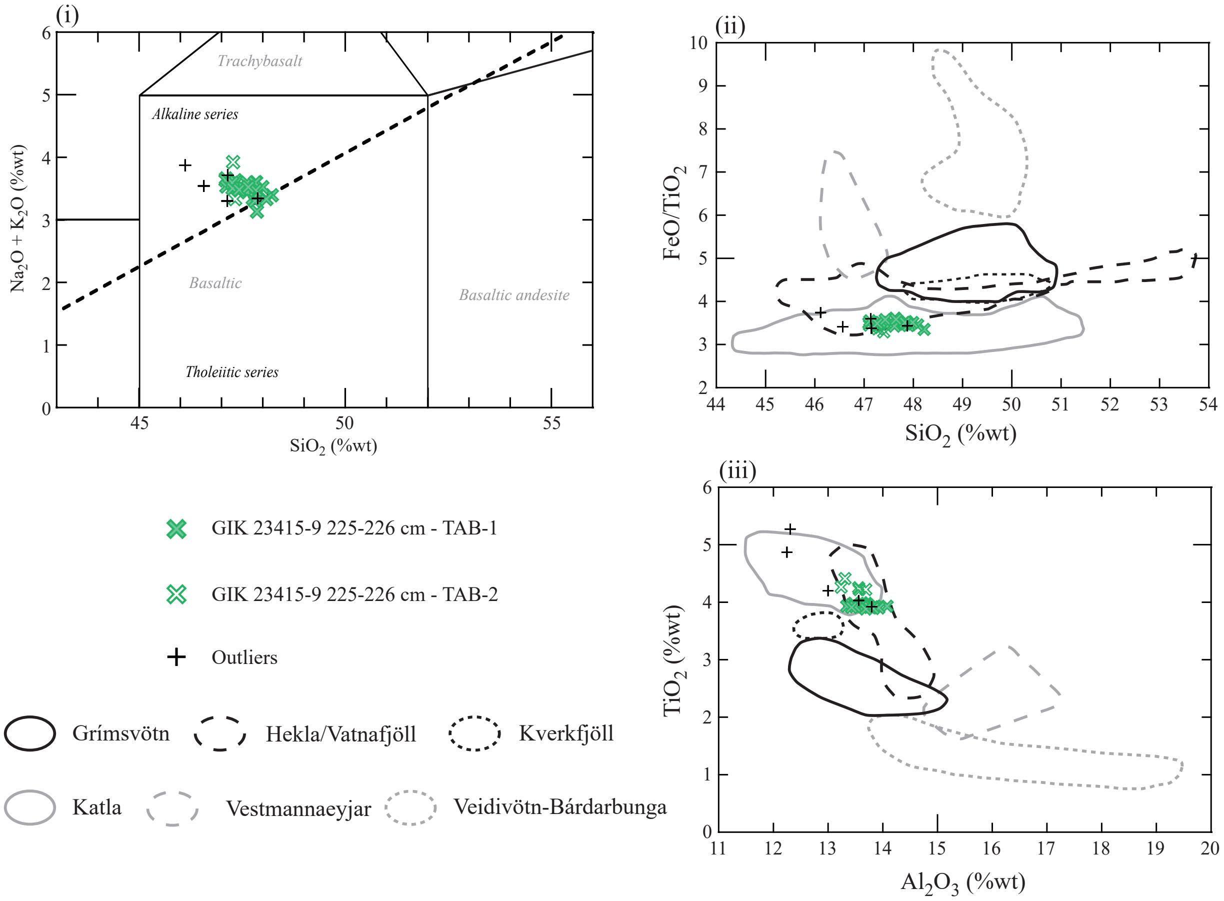

Figure S11: Geochemical populations identified within shard analyses from the GIK23415-9 225-226 cm deposit. (i) inset of total alkali vs. silica plot. Division line to separate alkaline and sub-alkaline material from MacDonald and Katsura (1964). Chemical classification and nomenclature after Le Maitre et al. (1989). (ii) FeO/TiO_2 vs. SiO_2 and (iii) TiO_2 vs. Al_2O_3 compositional variation diagrams comparing populations to characterisations of proximal Icelandic material. Geochemical fields for Icelandic source volcanoes are based on those utilised in Bourne et al. (2015) and references within.

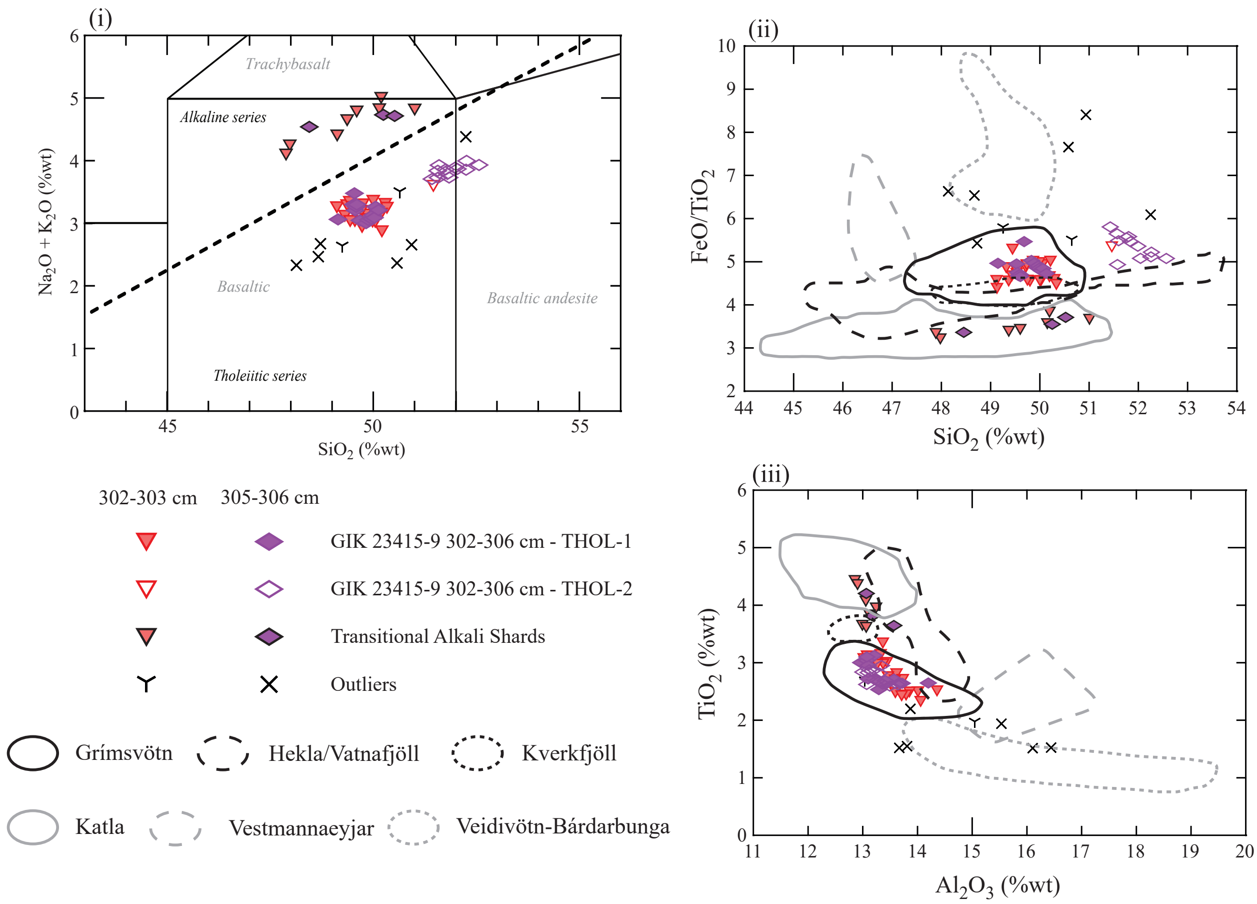

Figure S12: Geochemical populations identified within shard analyses from the GIK23415-9 302-306 cm deposit. (i) inset of total alkali vs. silica plot. Division line to separate alkaline and sub-alkaline material from MacDonald and Katsura (1964). Chemical classification and nomenclature after Le Maitre et al. (1989). (ii) FeO/TiO_2 vs. SiO_2 and (iii) TiO_2 vs. Al_2O_3 compositional variation diagrams comparing populations to characterisations of proximal Icelandic material. Geochemical fields for Icelandic source volcanoes are based on those utilised in Bourne et al. (2015) and references within.

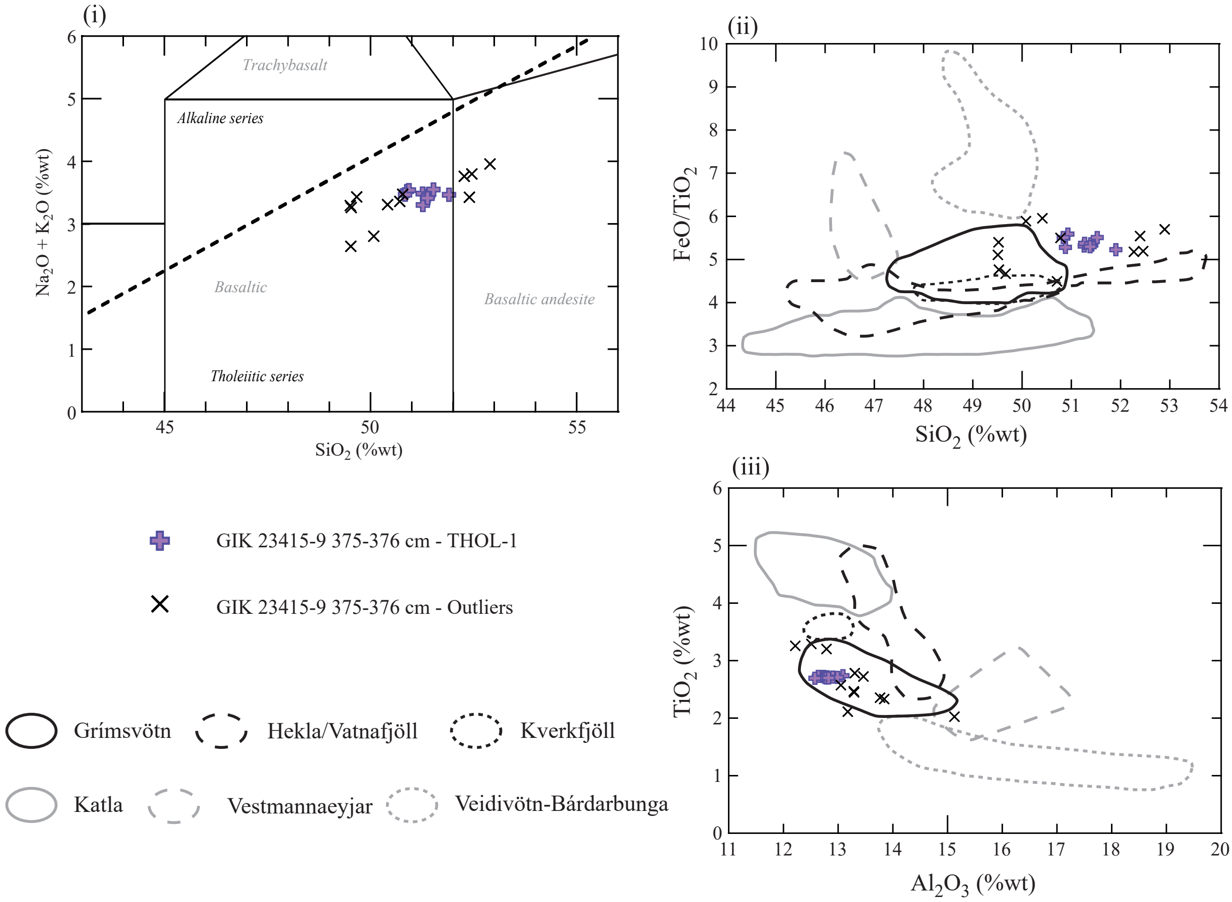

Figure S13: Geochemical populations identified within shard analyses from the GIK23415-9 375-376 cm deposit. (i) inset of total alkali vs. silica plot. Division line to separate alkaline and sub-alkaline material from MacDonald and Katsura (1964). Chemical classification and nomenclature after Le Maitre et al. (1989). (ii) FeO/TiO_2 vs. SiO_2 and (iii) TiO_2 vs. Al_2O_3 compositional variation diagrams comparing populations to characterisations of proximal Icelandic material. Geochemical fields for Icelandic source volcanoes are based on those utilised in Bourne et al. (2015) and references within.